UCRL-ID-144933

LLNL Modeling Calculations in Support of the CLP Program: FY01 3Q Report

M. Gerassimenko

July 26, 2001

U.S. Department of Energy

Lawrence
Livermore
National
Laboratory

Approved for public release; further dissemination unlimited

DISCLAIMER

This document was prepared as an account of work sponsored by an agency of the United States Government. Neither the United States Government nor the University of California nor any of their employees, makes any warranty, express or implied, or assumes any legal liability or responsibility for the accuracy, completeness, or usefulness of any information, apparatus, product, or process disclosed, or represents that its use would not infringe privately owned rights. Reference herein to any specific commercial product, process, or service by trade name, trademark, manufacturer, or otherwise, does not necessarily constitute or imply its endorsement, recommendation, or favoring by the United States Government or the University of California. The views and opinions of authors expressed herein do not necessarily state or reflect those of the United States Government or the University of California, and shall not be used for advertising or product endorsement purposes.

This work was performed under the auspices of the U. S. Department of Energy by the University of California, Lawrence Livermore National Laboratory under Contract No. W-7405-Eng-48.

This report has been reproduced directly from the best available copy.

Available electronically at http://www.doc.gov/bridge

Available for a processing fee to U.S. Department of Energy
And its contractors in paper from
U.S. Department of Energy
Office of Scientific and Technical Information
P.O. Box 62
Oak Ridge, TN 37831-0062
Telephone: (865) 576-8401
Facsimile: (865) 576-5728
E-mail: reports@adonis.osti.gov

Available for the sale to the public from
U.S. Department of Commerce
National Technical Information Service
5285 Port Royal Road
Springfield, VA 22161
Telephone: (800) 553-6847
Facsimile: (703) 605-6900
E-mail: orders@ntis.fedworld.gov
Online ordering: http://www.ntis.gov/ordering.htm

OR

Lawrence Livermore National Laboratory
Technical Information Department's Digital Library
http://www.llnl.gov/tid/Library.html

Introduction

A program to examine equation-of-state (EOS) issues of interest to the Corporate Lethality Program within the Ballistic Missile Defense Organization is getting underway. There are current plans to conduct experiments at Sandia National Laboratory in Albuquerque. The initial experiments will be two-dimensional: a thin flyer will normally impact a target at two nominal velocities 6 km/s and 11 km/s. A witness plate is placed parallel to the target, separated from it by a 75 mm gap. Several channels of VISAR measure the particle velocity at different locations at the rear of the witness plate. A schematic of the experimental configuration is shown in Figure 1.

At a kick-off meeting in March 2001, the initial computational task for all three laboratories (SNLA, LANL, and LLNL) was to calculate the witness plate particle velocity profiles produced by the two contemplated projectile sizes at both projectile velocities and to examine the effect of increasing the target to witness plate gap. This report documents these calculations as well as further calculations prompted by the initial results.

First Series of Modeling Calculations

Calculations setup

Modeling calculations are done with the CALE code, which is a 2-D axisymmetric hydrodynamics code with arbitrary Lagrange Eulerian capabilities. In these calculations, there is an axis of rotational symmetry located at zero in the radial direction. Physically, zones are hoops whose axis is this rotational symmetry axis. Many figures in this report are cross sections with the rotational symmetry axis running left to right. The radial coordinate (r) is up down, the axial coordinate z is left right. The calculation setup for a 12.7 mm diameter projectile is shown in Figure 2. The rotational symmetry axis at r=0 and zoning is indicated in the upper half. The projectile, target and witness plate appear as rectangles, but this is a cross section so they are physically thin cylinders. Zoning is difficult to see for the projectile, target and witness plate, it is better visible in the close-ups shown in Figures 3 and 4. The calculational setup and close up for a 17 mm diameter projectile are shown in Figures 5 and 6. Tracer points that move with the material are located at the rear of the witness plate on axis and at 2 mm intervals radially.

Standard zoning is 140x113 zones along the axis and radius, respectively. This amounts to 9 zones across the thickness of the projectile 10 zones across the thickness of the target and the witness plate, the target and the witness plate as well as 100 zones across the 75 mm gap between the target and the witness plate. Radially zoning is close to uniform with 9 zones across the 6.35 mm radius projectile and 12 across the 8.5 mm radius one.

The background material is vacuum with a density of 10^{-6} g/cm^3. The projectile EOS is a Gruneisen one with coefficients determined for TI6Al4V which is the titanium alloy the projectile is made of. The target EOS is a tabular one, referred to as LEOS at LLNL, which treats all phases of materials. The witness plate EOS is a polynominal one with coefficients determined for the 6061-T6 aluminum alloy. All material constitutive models are elastic plastic. Material failure (zero strength) takes place when the tensile strength is exceeded in tension or when the accumulated effective plastic strain exceeds the maximum specified in the EOS. Material parameters are listed in Table 1.

Table 1
Material Parameters

Projectile:	Gruneisen EOS for Ti6Al4V alloy density = 4.419 g/cm^3 coefficients c=0.513, S1=1.028, S2=0, S3=0, G0=1.23, A=0.17 modulus = 419 kbars, yield strength = 13.2 kbars maximum effective plastic strain = 2 tensile strength = 25 kbars
Target:	LEOS for aluminum (LEOS 130) density = 2.70 g/cm^3 modulus = 276 kbars, yield strength = 2.9 kbars no effective plastic strain based failure tensile strength = 12 kbars
Witness plate:	polynomial EOS for 6061 T6 aluminum alloy density = 2.703 g/cm^3 coefficients A0=0, AP=0.742179, A2=0.604876, A3=0.187029, B0=1.97, B1=0.48, B3=0 modulus = 276 kbars, yield strength = 2.9 kbars maximum effective plastic strain = 0.5 tensile strength = 12 kbars

Results of the Calculations

Results of the modeling calculations for a 12.7 mm diameter projectile at 6 km/s initial velocity are shown in Figures 7 and 8. Figure 7 is a materials map at the end of the calculation with zoning indicated above the symmetry axis. The particle velocity profiles, at the rear of the witness plate, on axis and 2, 4, and 6 mm away are shown in Figure 8. Analogous results for a 17 mm diameter projectile are shown in Figures 9 and 10. Analogous results for an initial projectile velocity of 11 km/s are shown in Figures 11 through 14.

Examination of the results reveals severe damage and perforation of the witness plate near the axis. It is also evident that the particle velocity peaks are substantially higher for the 17 mm diameter projectile compared to the 12.7 mm diameter one.

We performed calculations with the gap between the target and witness plate increased from 75 mm to 100 and 150 mm. In these calculations, the zone size in the gap was kept the same by increasing the total number of zones in the problem. Zoning across the thickness of the projectile target and witness plate, as well as in the radial direction, was left unchanged.

Results of the modeling calculation for a 12.7 mm diameter projectile at 6 km/s initial velocity with a 100 mm gap are shown in Figures 15 and 16. Figure 15 is a materials map at the end of the calculation with zoning indicated above the symmetry axis. The particle velocity profiles, at the rear of the witness plate, or axis and 2, 4, and 6 mm away are shown in Figure 16. Analogous results for a 17 mm diameter projectile are shown in Figures 17 and 18. Analogous results for an 11 km/s initial projectile velocity are shown in Figures 10 through 22. Analogous results for a 17 mm diameter projectile with a 150 mm gap are shown in Figures 23 and 24 for a 6 km/s initial projectile velocity, and in Figures 25 and 26 for an 11 km/s initial projectile velocity.

Calculated particle velocity profiles for a 12.7 mm projectile at 6 km/s initial velocity for 75 mm and 100 mm gaps are compared in Figure 27. The profiles are essentially identical. The profiles are produced by impact upon this witness plate of a target fragment launched by projectile impact. In an experiment, we expect the fragments produced by projectile impact to be small, and to have a substantial velocity component in the plane normal to the projectile velocity. This would make the particle velocity profile dependent on gap size. Calculated particle velocity profiles for a 12.7 mm projectile at 11 km/s initial velocity for 75 mm and 100 mm gaps are compared in Figure 28. There are substantial differences in the calculated profiles.

Calculated particle velocity profiles for a 17 mm projectile at 6 km/s initial projectile velocity for 75, 100, and 150 mm gaps are shown in Figure 29. Analogous results for a 11 km/s initial projectile velocity are shown in Figure 30. There are differences in the calculated profiles.

Second Series of Modeling Calculations

We only consider a 75 mm gap, and to increase the meaningful length of the particle velocity record, we back the witness plate with a 10 mm thick LiF window. It is well known that the shock impedance of LiF is nearly identical to that of aluminum. We also restrict our attention to 17 mm diameter projectiles. Finally, we examine the effect of zoning on the calculated particle velocity profiles.

The model setup and close-ups with zoning are shown in Figures 31 through 33. Results for 6 km/s initial projectile velocity are shown in Figures 34 and 35, and Figures 36 and 37 for 11 km/s initial projectile velocity.

We examine the effect of resolution by increasing zoning from standard (150x113 zones) to fine (240x225 zones) and very fine (405x337 zones). In fine zoning, we keep the same number of zones across the thickness of the projectile, target, witness plate and backing, but increase it by a factor of two across the gap and in the radial direction. In very fine zoning, the number of zones is increased to 15 across the projectile thickness, to 20 across the target and witness plate, to 40 across the LiF thickness and by a factor of 3, relative to standard zoning, in the radial direction.

The model setup and close-ups with zoning for the fine zoning calculations are shown in Figures 38 through 40. Material plot at the end of the calculation and velocity profiles near axis at the witness plate/LiF interface are shown in Figures 41 and 42 for a 6 km/s initial projectile velocity. Analogous results for a 11 km/s initial projectile velocity are shown in Figures 43 and 44.

Close-ups with zoning for the very fine zoning calculations are shown in Figures 45 and 46. Material plot at the end of the calculation and velocity profiles near axis at the witness plate/LiF interface are shown in Figures 47 and 48 for a 6 km/s initial projectile velocity. Analogous results for a 11 km/s initial projectile velocity are shown in Figures 49 and 50. The calculated particle velocity profiles show substantial zoning dependence. The calculated particle velocity profiles on axis for a 6 km/s initial projectile velocity are compared for the three different zoning calculations in Figure 51. The timing of the profile first rise is very clearly zoning dependent: the finer the zoning the earlier the first rise. The calculated particle profiles on axis for a 11 km/s initial projectile velocity are compared for the three different zoning in Figure 52. The timing of the profiles shows the same zoning dependence noted earlier. The very fine zoning calculation actually resolves the debris cloud into four separate chunks which arrive over 2 μs. In an experiment, we expect the fragments produced by projectile impact to be small, so there should be a smooth distribution of particles arriving over a period of time on the witness plate.

Validation Experiments: Simple 2-D

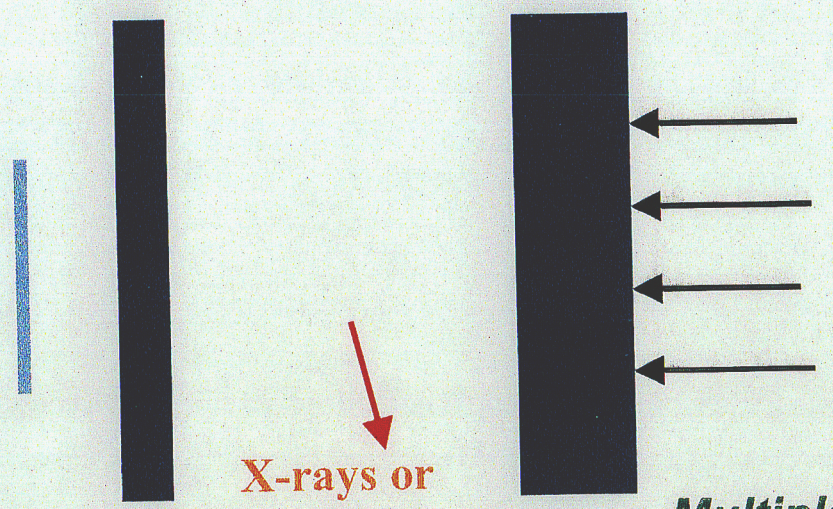

Experimental Configuration:
Three-Stage Gun: 6 and 11 km/s
0.8 mm Flyer - Ti-6Al-4V
2.5 mm Aluminum Target
4 mm Witness Plate Aluminum
75, 100, or 150 mm Spacing

Multiple VISAR recording on witness plate

Computational study addressing impulse structure on a backwall as a function of varying:

1) stand off distance

2) flier-plate diameter (12.7 mm vs 17 mm) for a fixed stand-off distance

Figure 1

First series CLP EOS experiments modeling calculations

12.7mm diameter projectile: materials plot and zoning

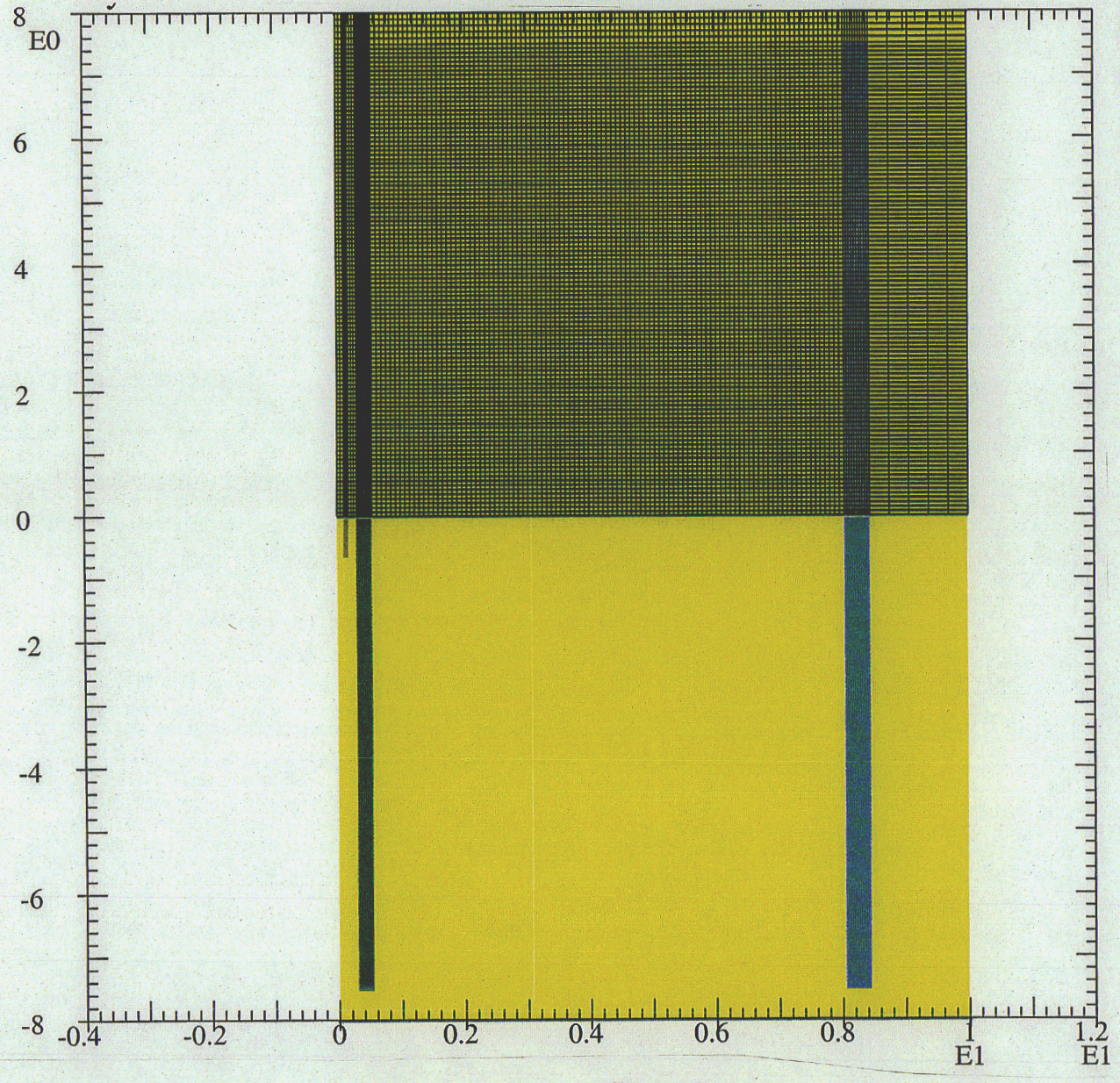

Red: projectile
Green: target
Blue: witness plate
Yellow: vacuum background

clpa--1-mg-6-19-2001

Figure 2

First series CLP EOS experiments modeling calculations

Closeup of 12.7mm diameter projectile: materials plot and zoning

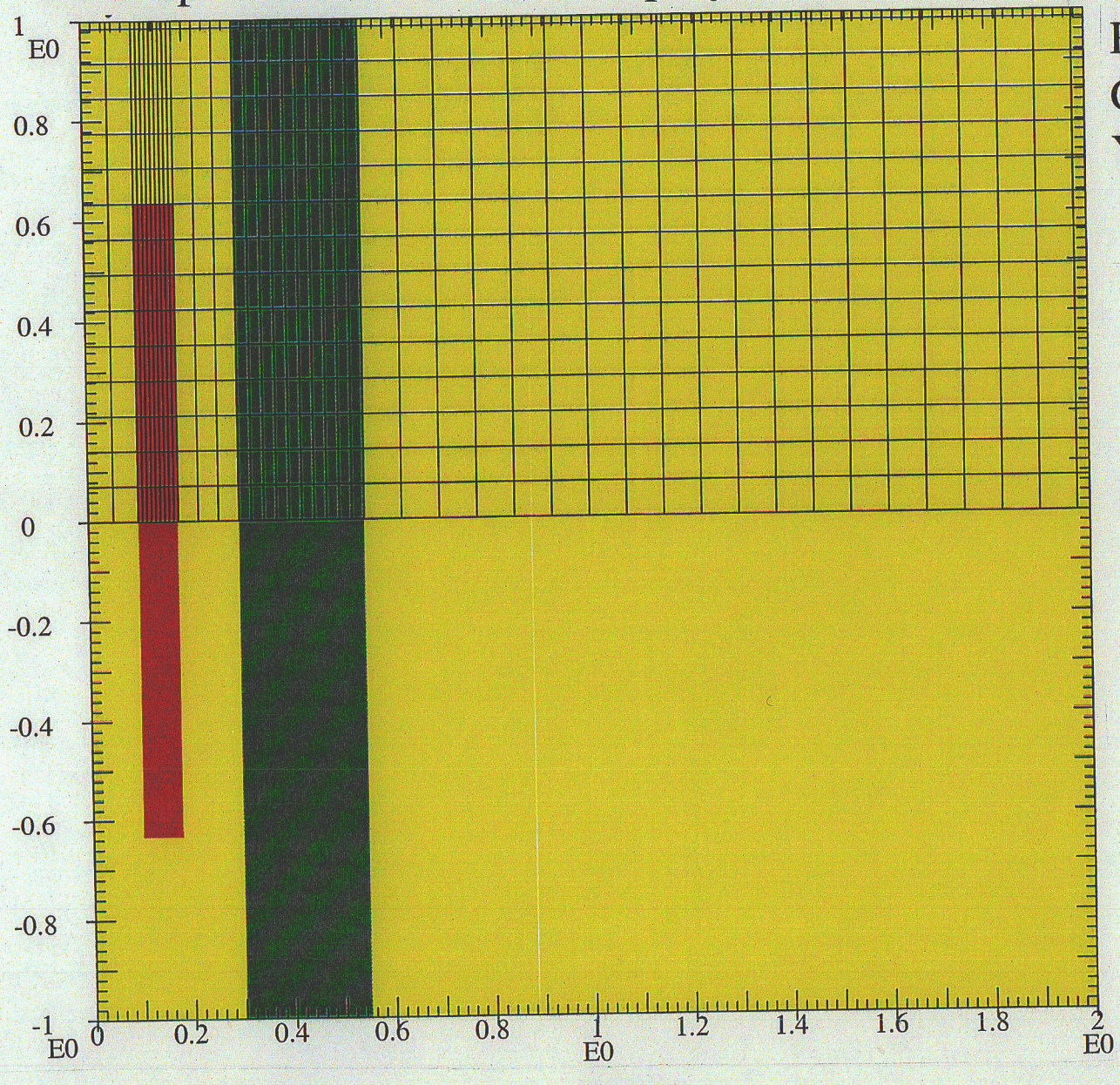

Red: projectile
Green: target
Yellow: vacuum background

clpa--3-mg-6-19-2001

Figure 3

First series CLP EOS experiments modeling calculations

Closeup of witness plate and gap: materials plot and zoning

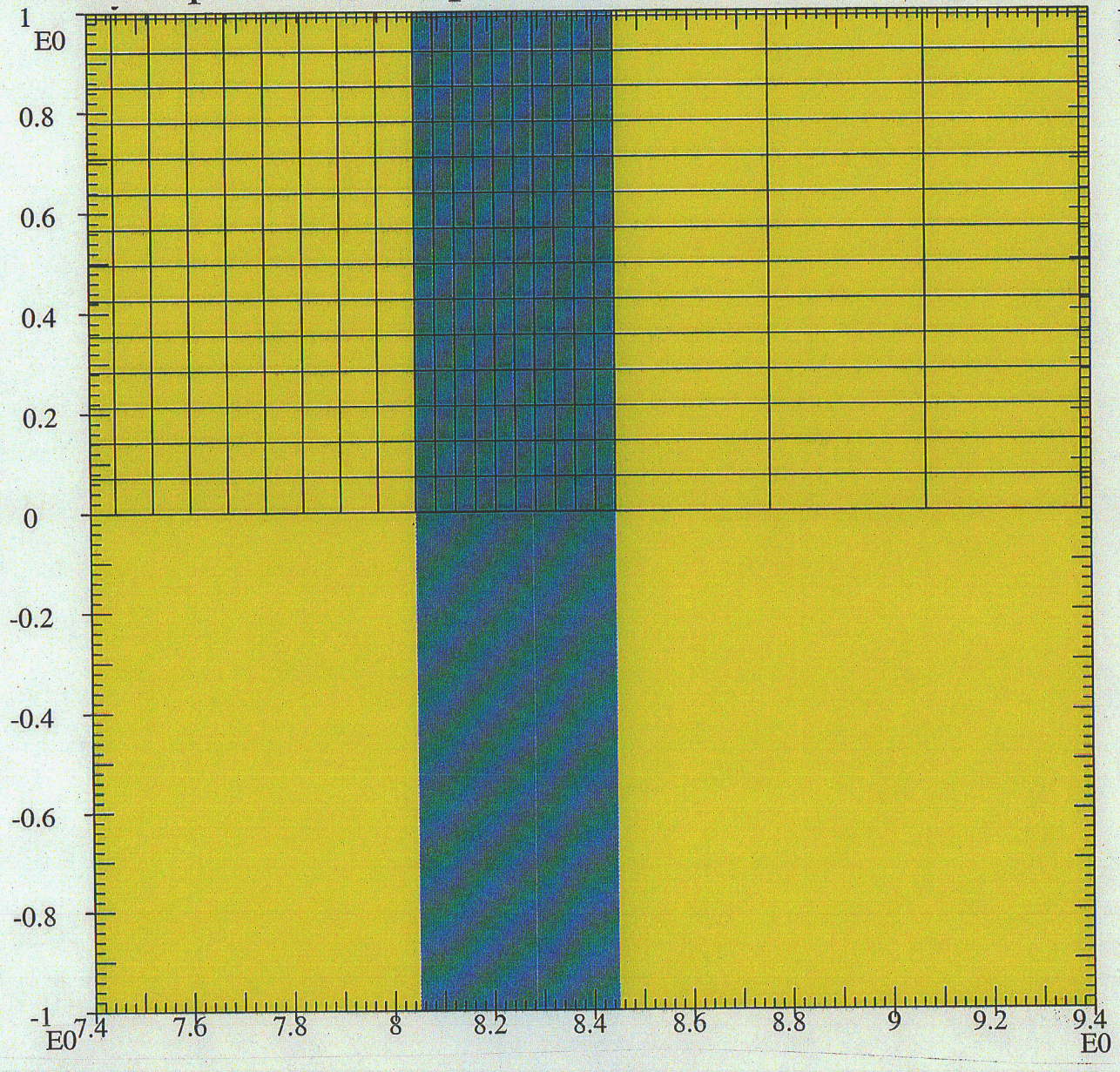

Blue: witness plate

Yellow: vacuum background

clpa--5-mg-6-19-2001

Figure 4

First series CLP EOS experiments modeling calculations

17mm diameter projectile: materials plot and zoning

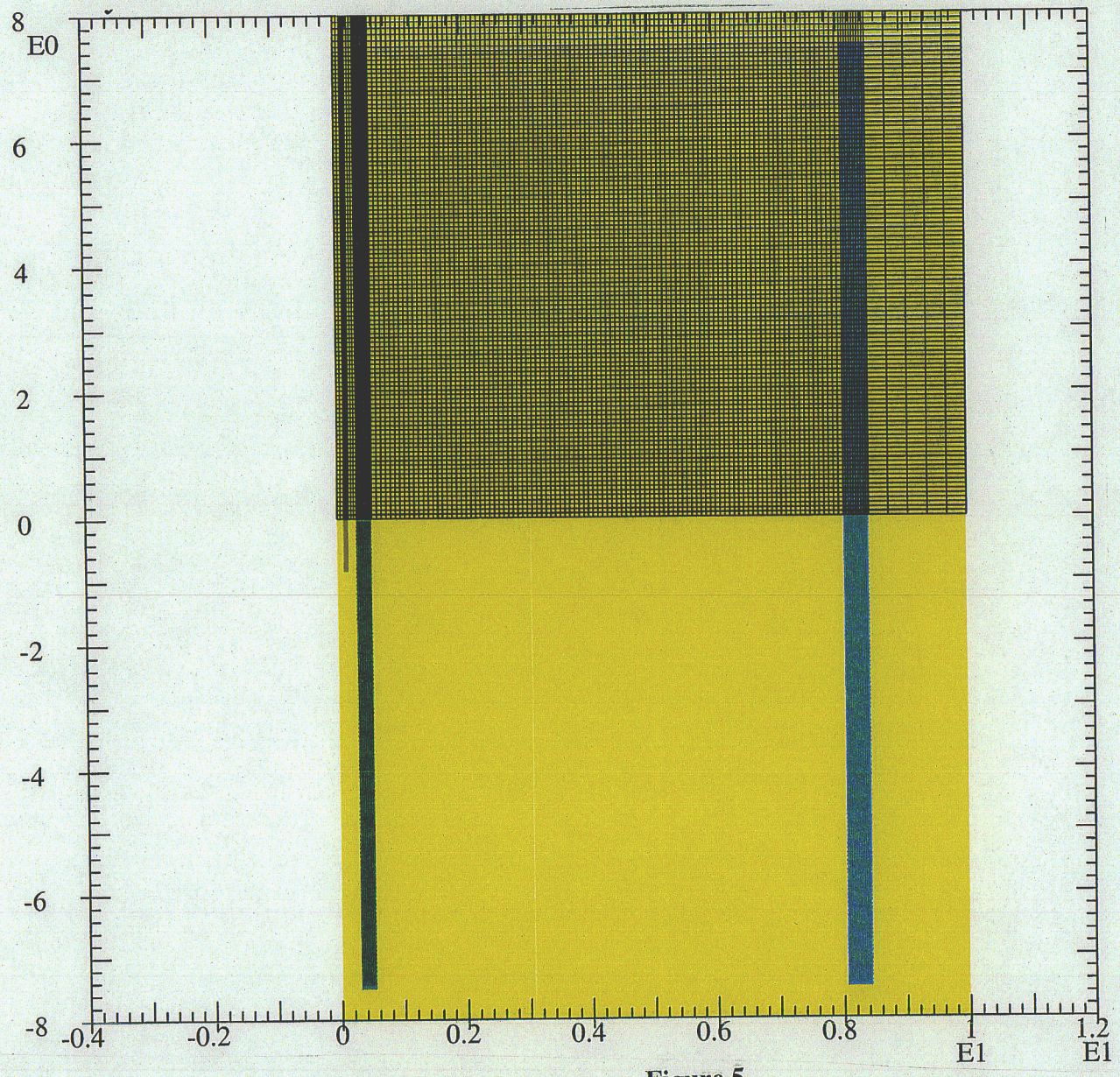

Red: projectile
Green: target
Blue: witness plate
Yellow: vacuum background

clpa--2-mg-6-19-2001

Figure 5

First series CLP EOS experiments modeling calculations

Closeup of 17mm diameter projectile: materials plot and zoning

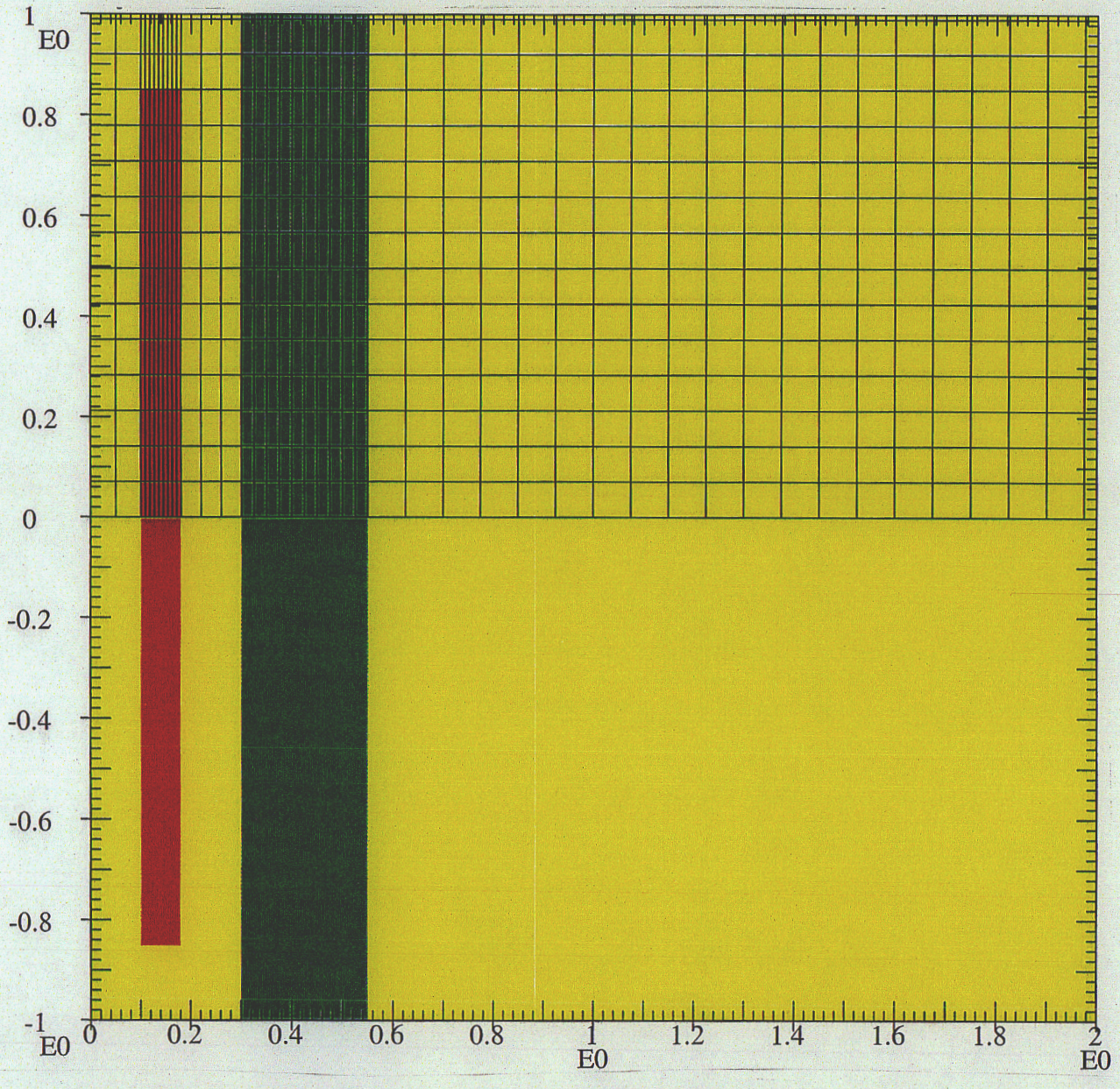

Red: projectile

Green: target

Yellow: vacuum background

clpa--4-mg-6-19-2001

Figure 6

First series CLP EOS experiments modeling calculations

12.7mm diameter projectile at 6km/s:t=20μs materials plot and zoning

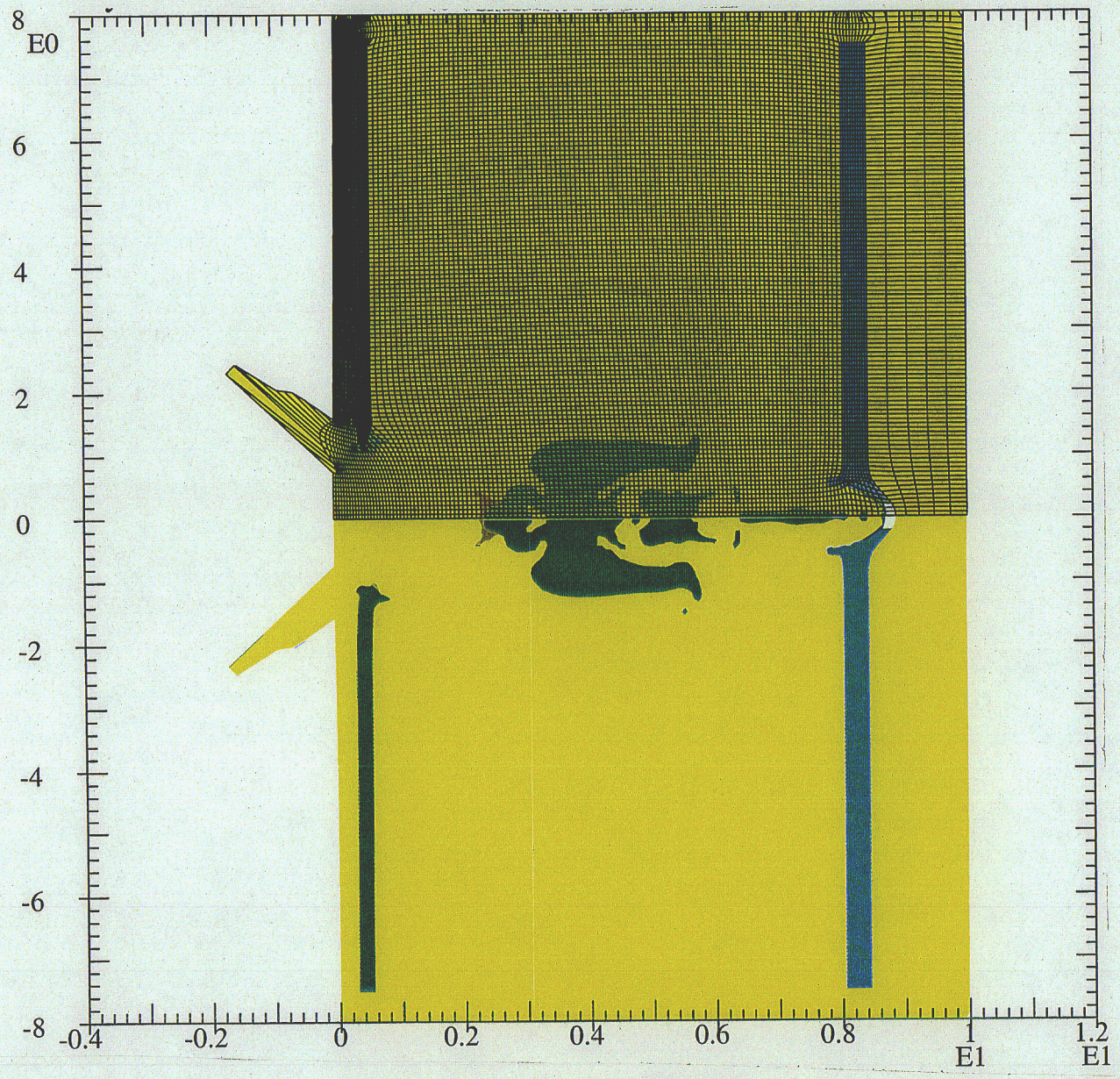

Red: projectile
Green: target
Blue: witness plate
Yellow: vacuum background

clpa--7-mg-6-18-2001

Figure 7

First series CLP EOS experiments modeling calculations

12.7mm diameter projectile at 6km/s: particle velocities at rear of witness plate on axis and 2,4 and 6mm away

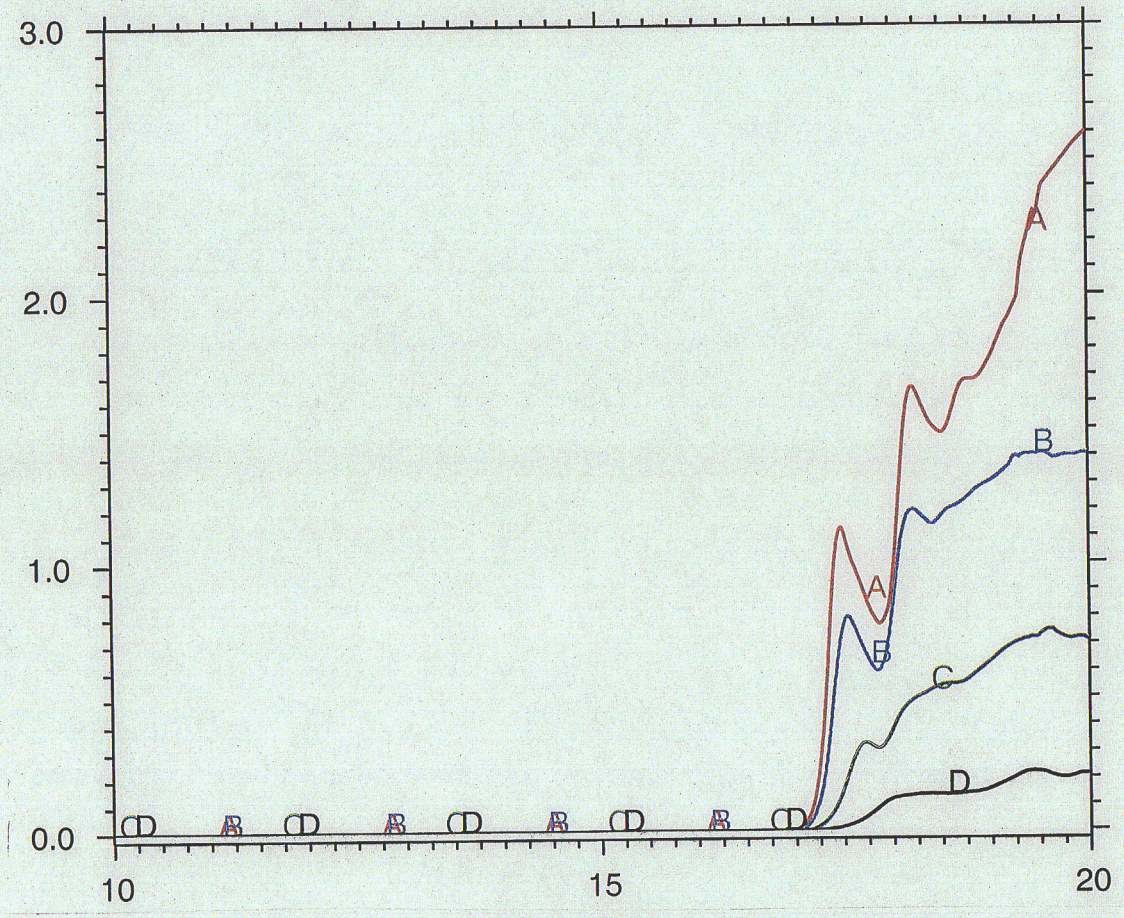

Figure 8

clpa--10-mg-6-19-2001

First series CLP EOS experiments modeling calculations

17mm diameter projectile at 6km/s:t=20μs materials plot and zoning

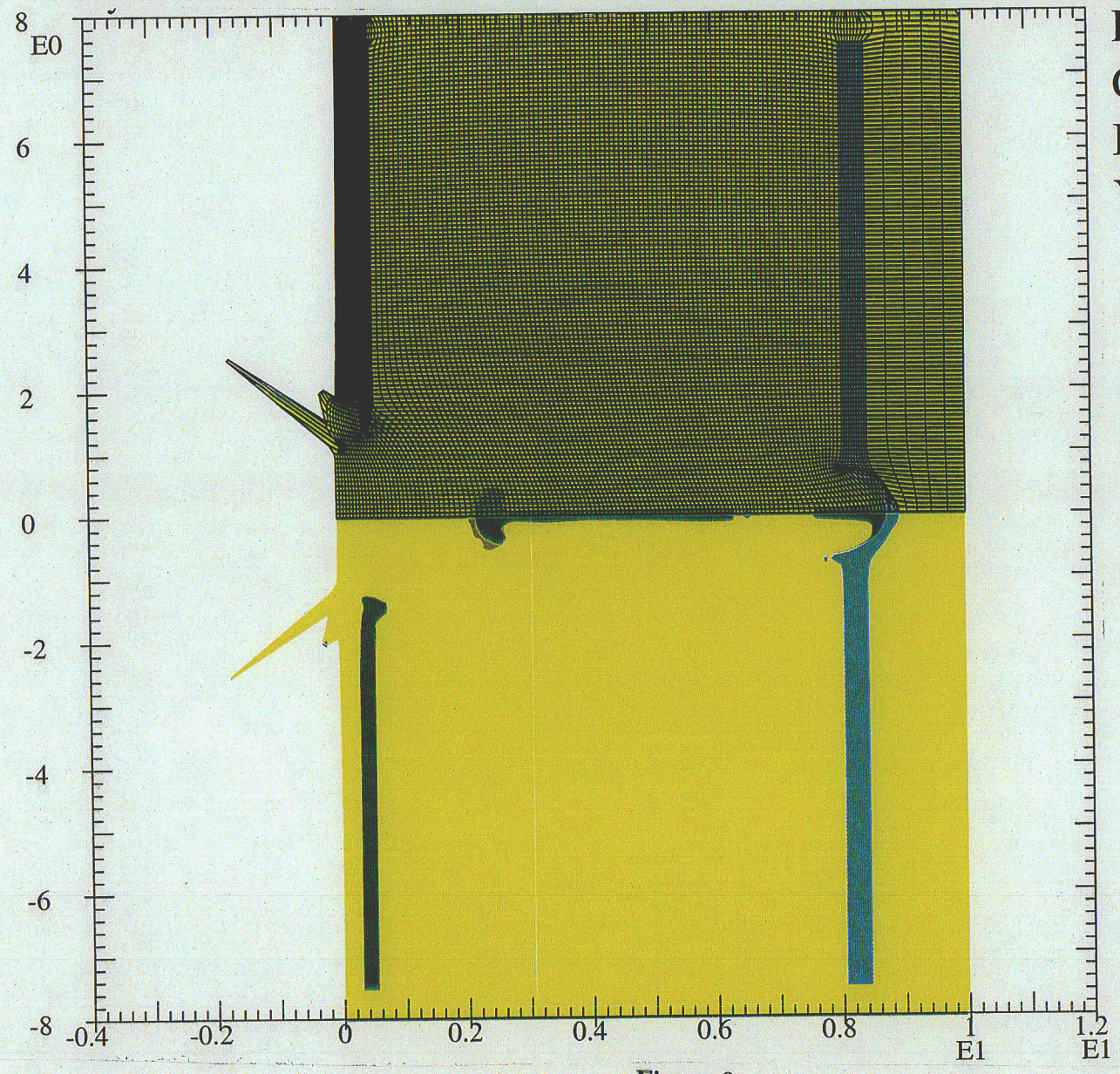

Red: projectile
Green: target
Blue: witness plate
Yellow: vacuum background

clpa--6-mg-6-18-2001

Figure 9

First series CLP EOS experiments modeling calculations

17mm diameter projectile at 6km/s: particle velocities at rear of witness plate on axis and 2,4 and 6mm away

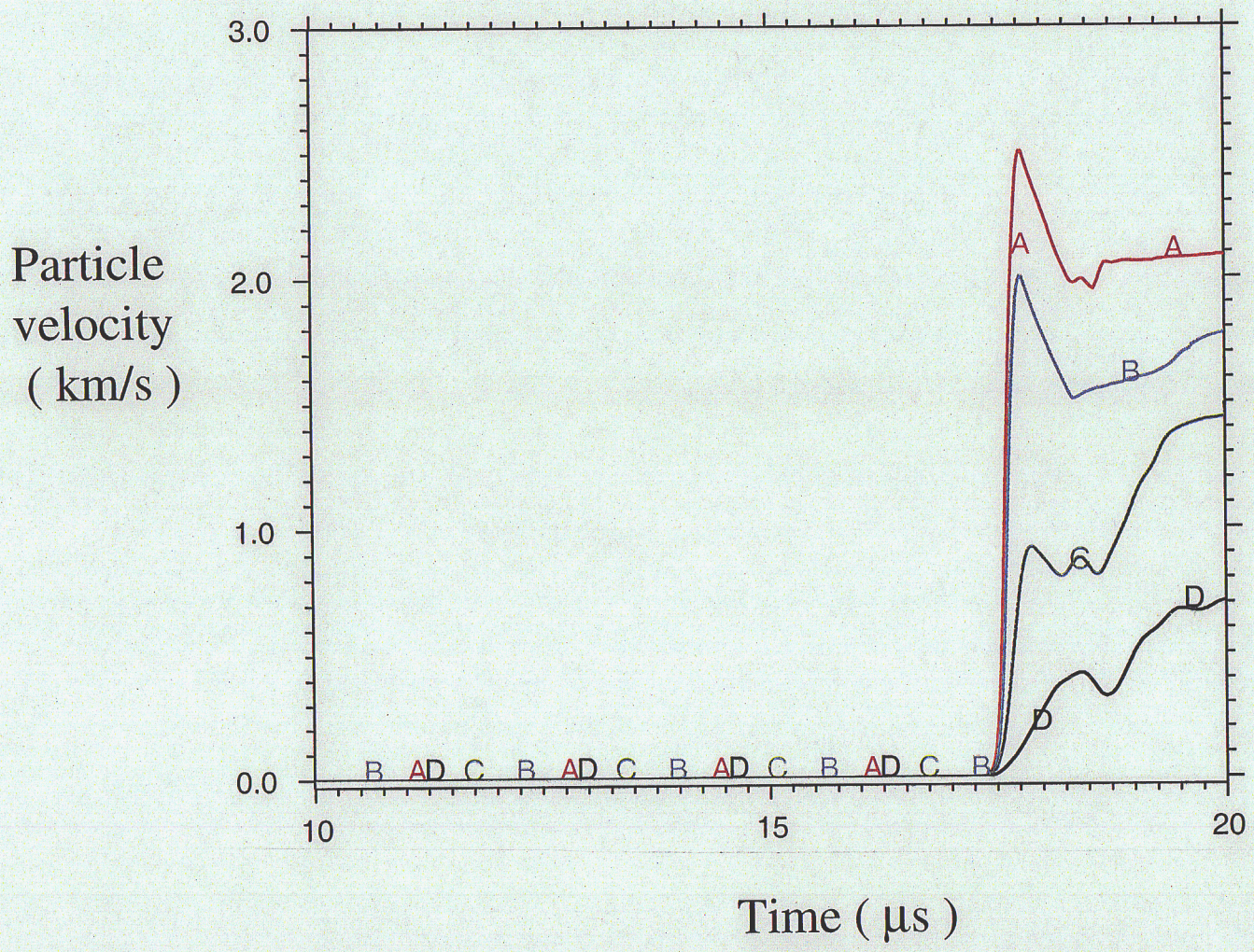

Figure 10

clpa--11-mg-6-19-2001

First series CLP EOS experiments modeling calculations

12.7mm diameter projectile at 11km/s:t=10.5μs materials plot and zoning

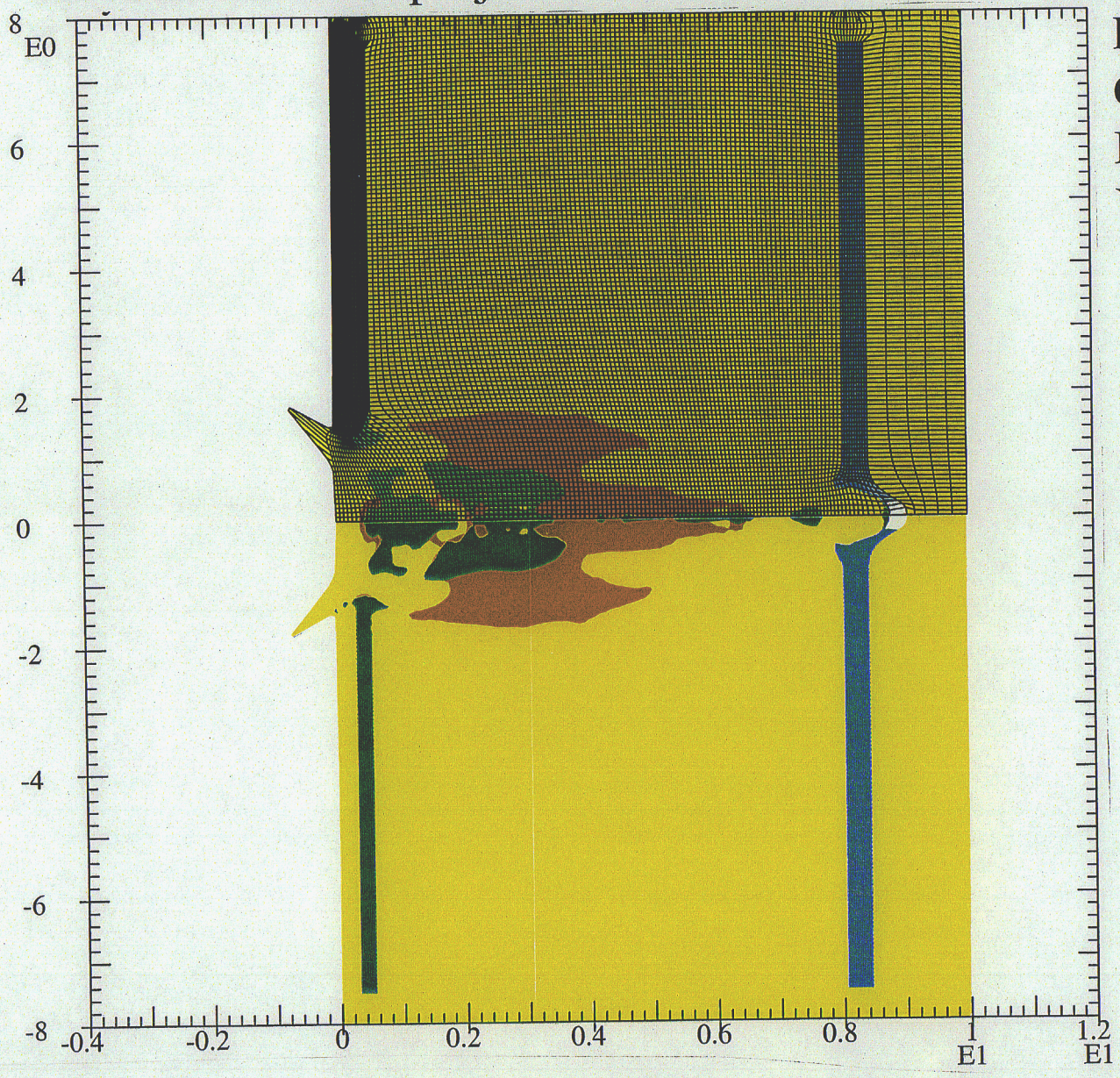

Red: projectile
Green: target
Blue: witness plate
Yellow: vacuum background

clpa--8-mg-6-18-2001

Figure 11

First series CLP EOS experiments modeling calculations

12.7mm diameter projectile at 11km/s: particle velocities at rear of witness plate on axis and 2,4 and 6mm away

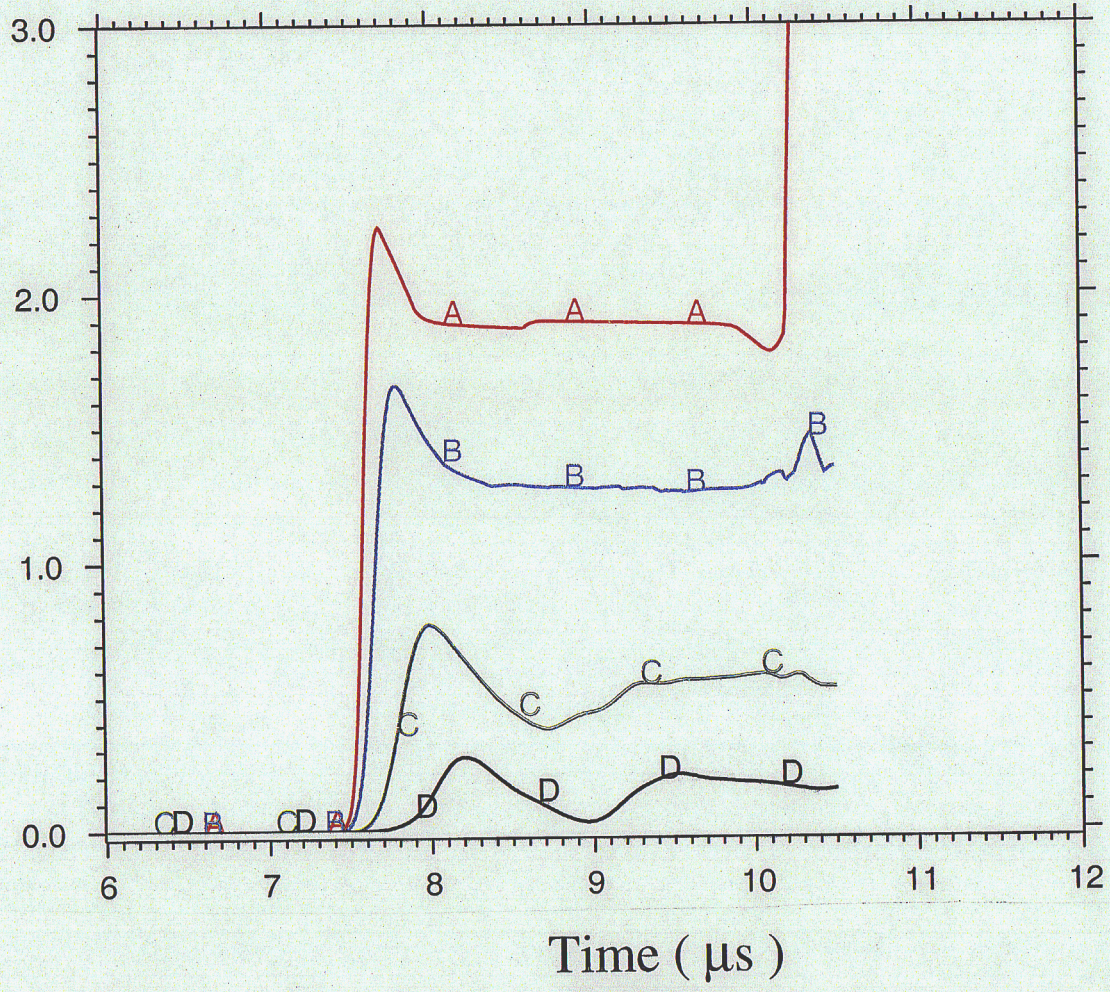

Figure 12

clpa--12-mg-6-19-2001

First series CLP EOS experiments modeling calculations

17mm diameter projectile at 11km/s:t=12μs materials plot and zoning

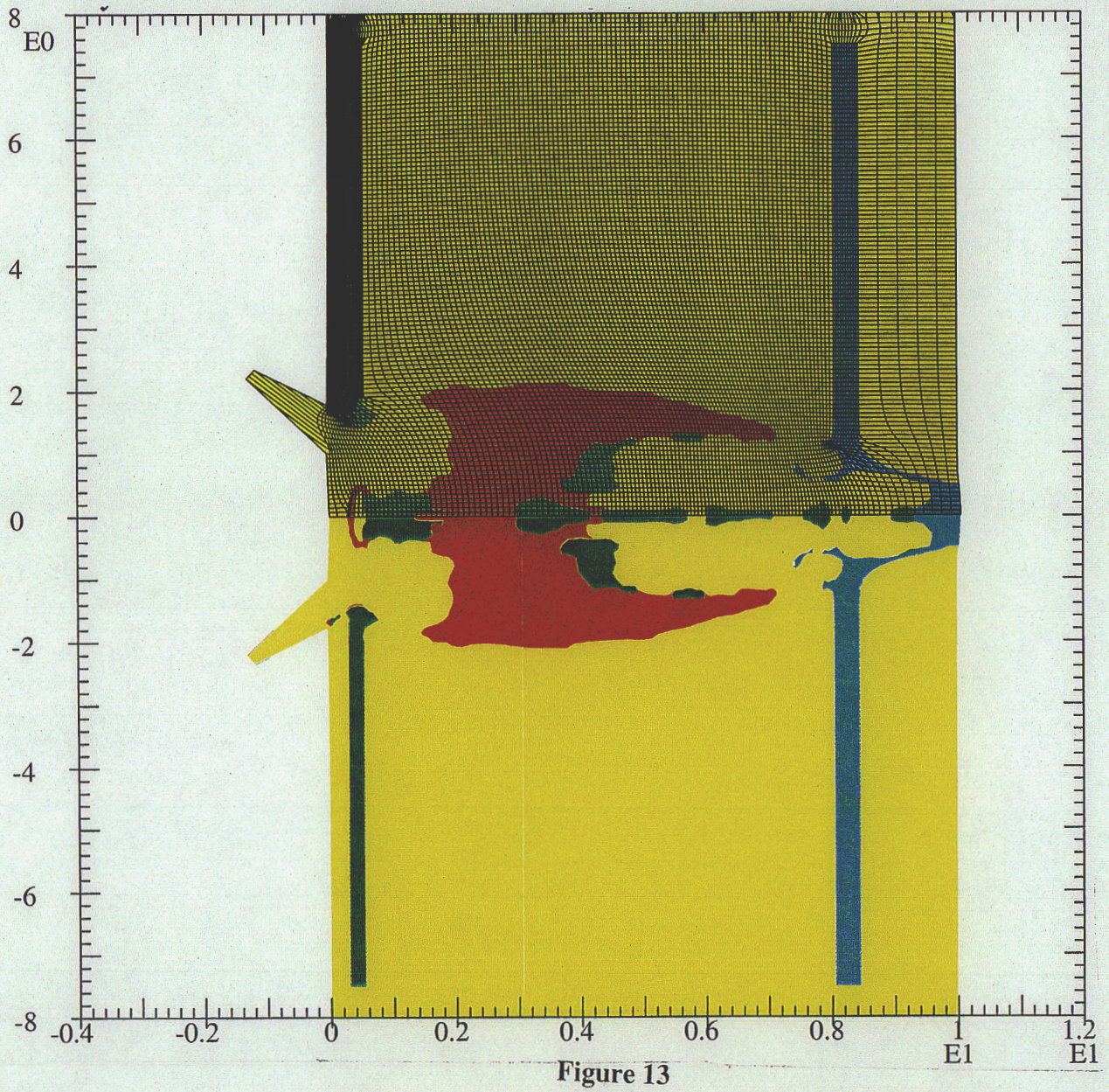

Red: projectile
Green: target
Blue: witness plate
Yellow: vacuum background

clpa--9-mg-6-18-2001

Figure 13

First series CLP EOS experiments modeling calculations

17mm diameter projectile at 11km/s: particle velocities at rear of witness plate on axis and 2,4 and 6mm away

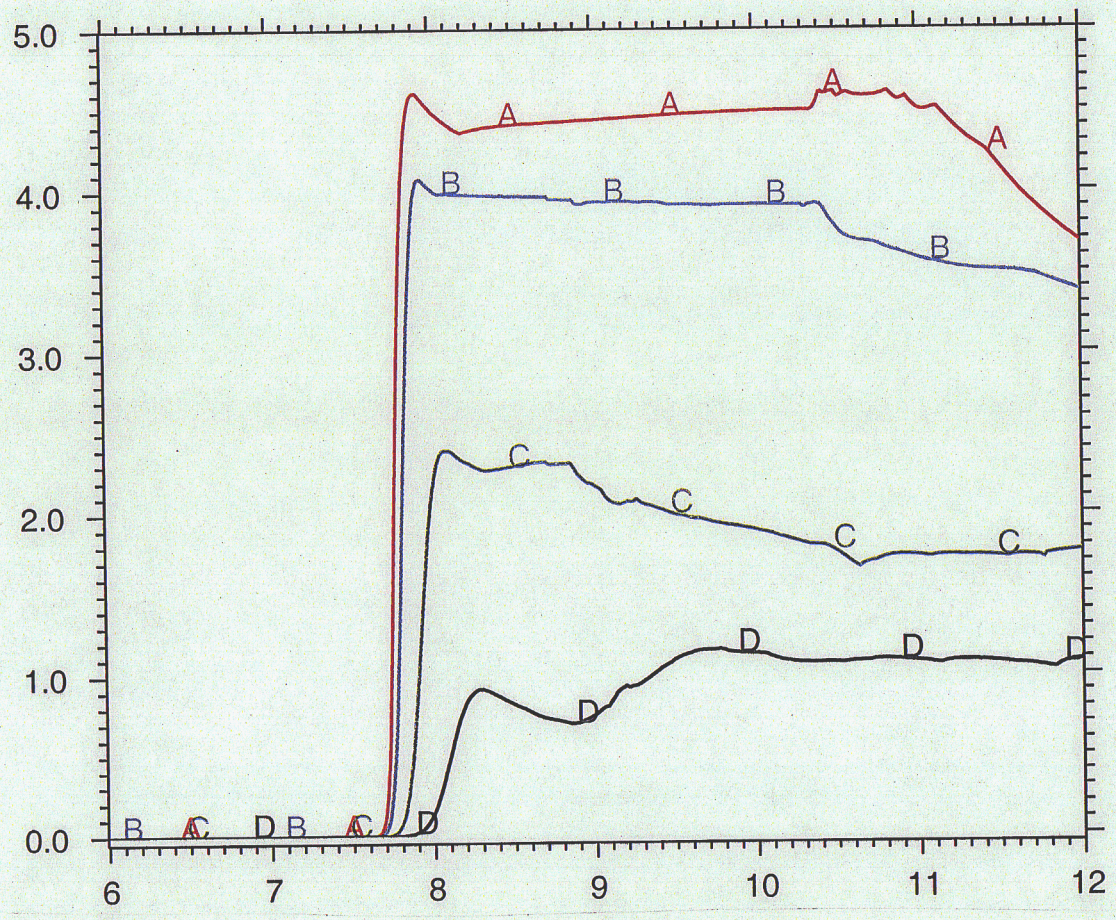

Figure 14

clpa--13-mg-6-19-2001

First series CLP EOS experiments modeling calculations

12.7mm dia. proj. at 6km/s 100mm gap: t=26μs mat. plot and zoning

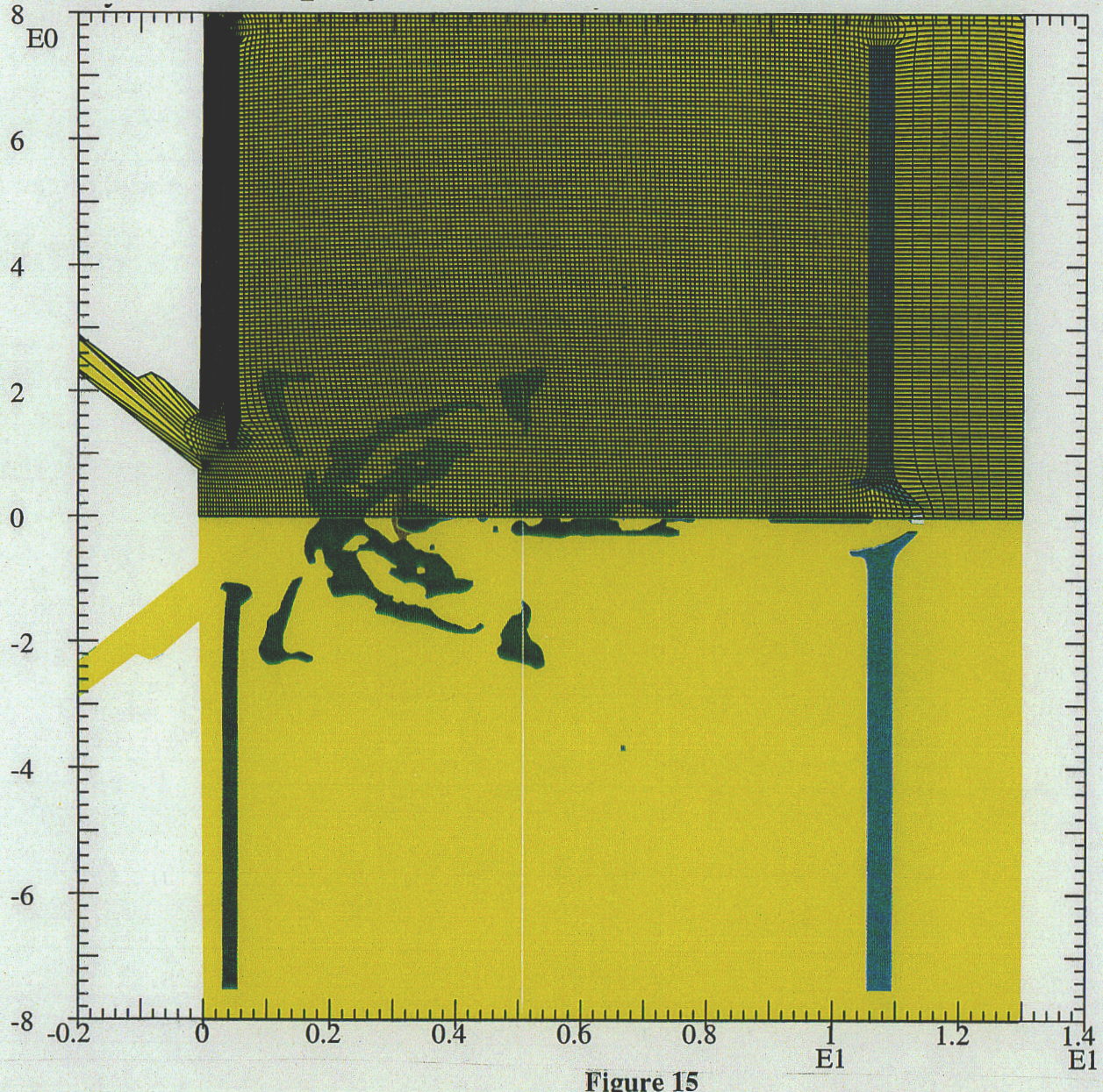

Red: projectile
Green: target
Blue: witness plate
Yellow: vacuum background

clpb--11-mg-7-12-2001

Figure 15

First series CLP EOS experiments modeling calculations

12.7mm diameter projectile at 6km/s 100mm gap: particle velocities at rear of witness plate on axis and 2,4 and 6mm away

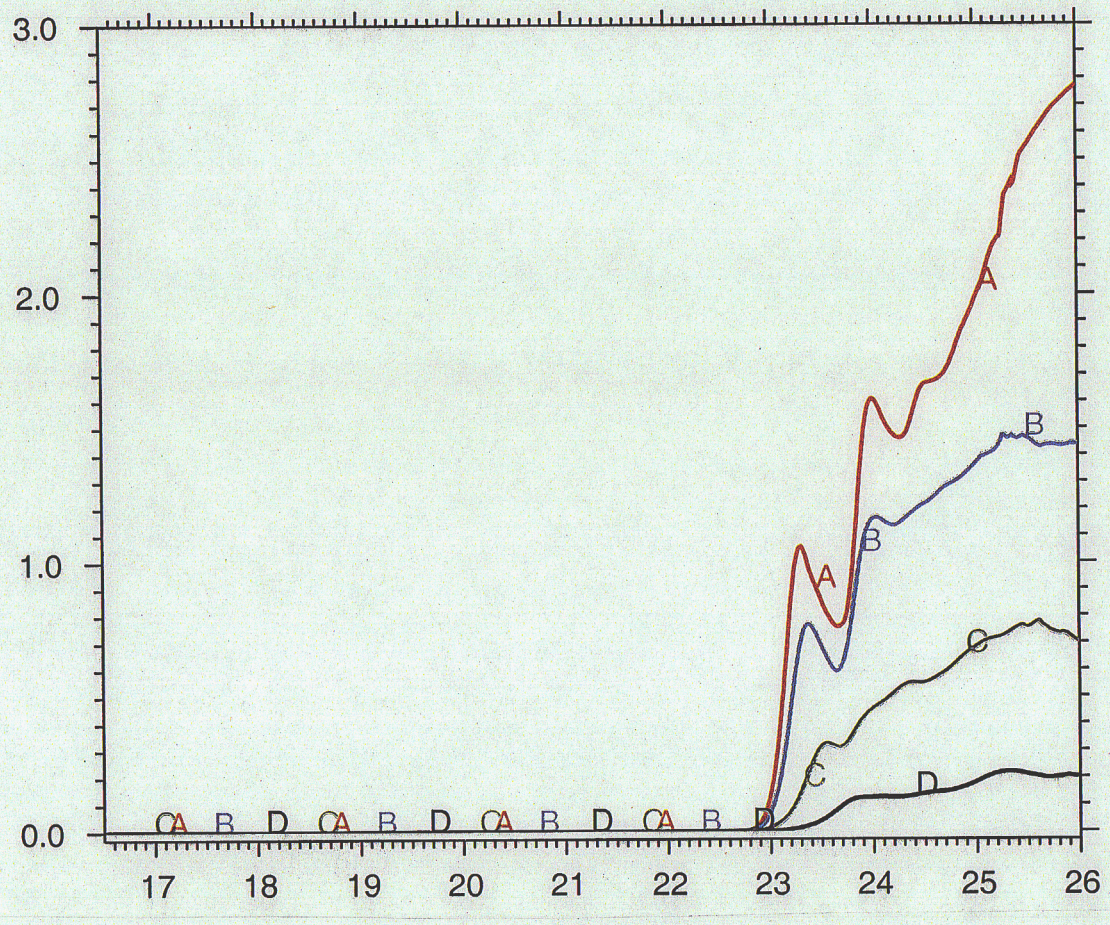

Figure 16

clpb--1-mg-7-11-2001

First series CLP EOS experiments modeling calculations

17mm dia. proj. at 6km/s 100mm gap: t=26μs mat. plot and zoning

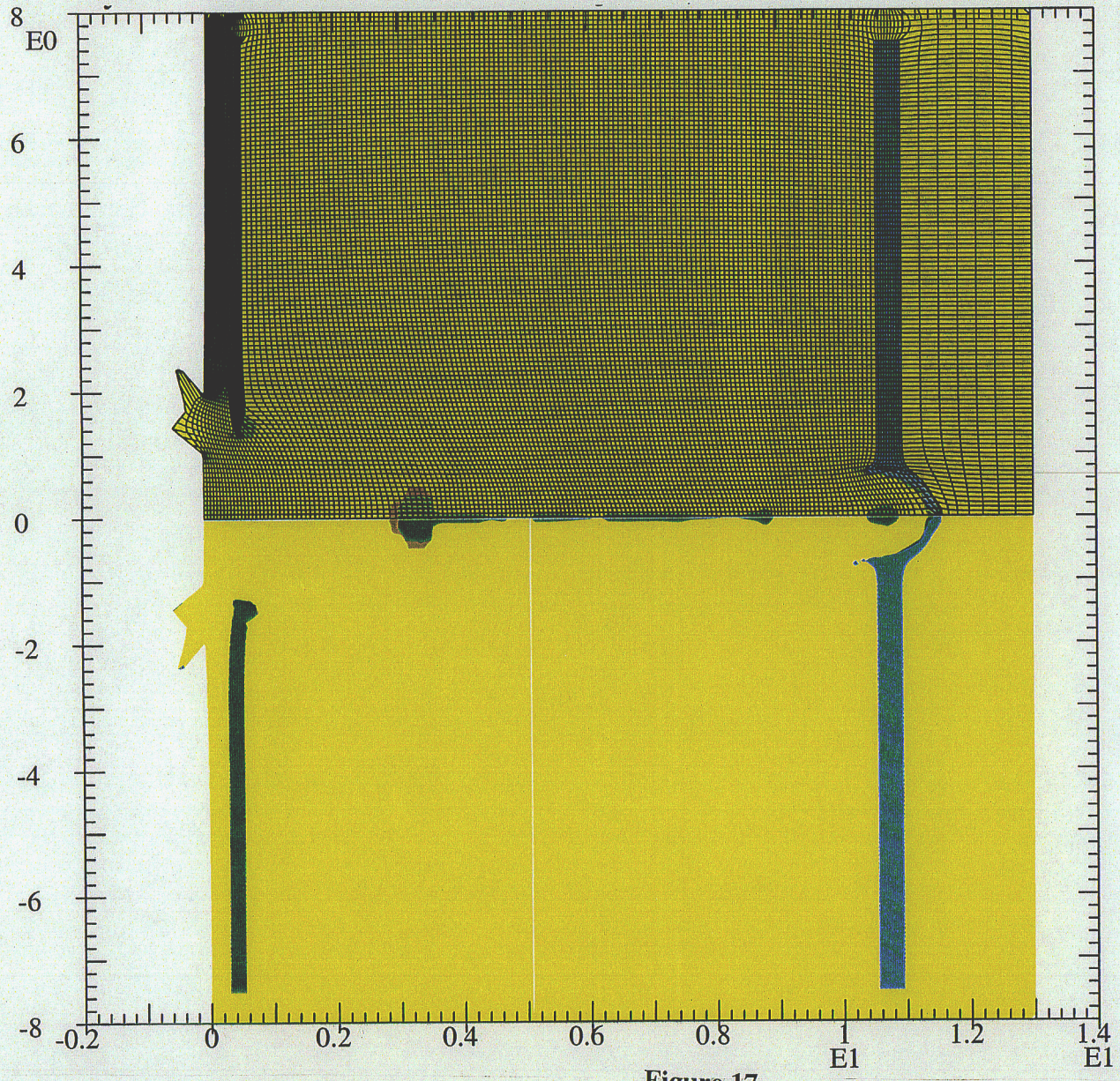

Red: projectile
Green: target
Blue: witness plate
Yellow: vacuum background

clpb--12-mg-7-12-2001

Figure 17

First series CLP EOS experiments modeling calculations

17mm diameter projectile at 6km/s 100mm gap: particle velocities at rear of witness plate on axis and 2,4 and 6mm away

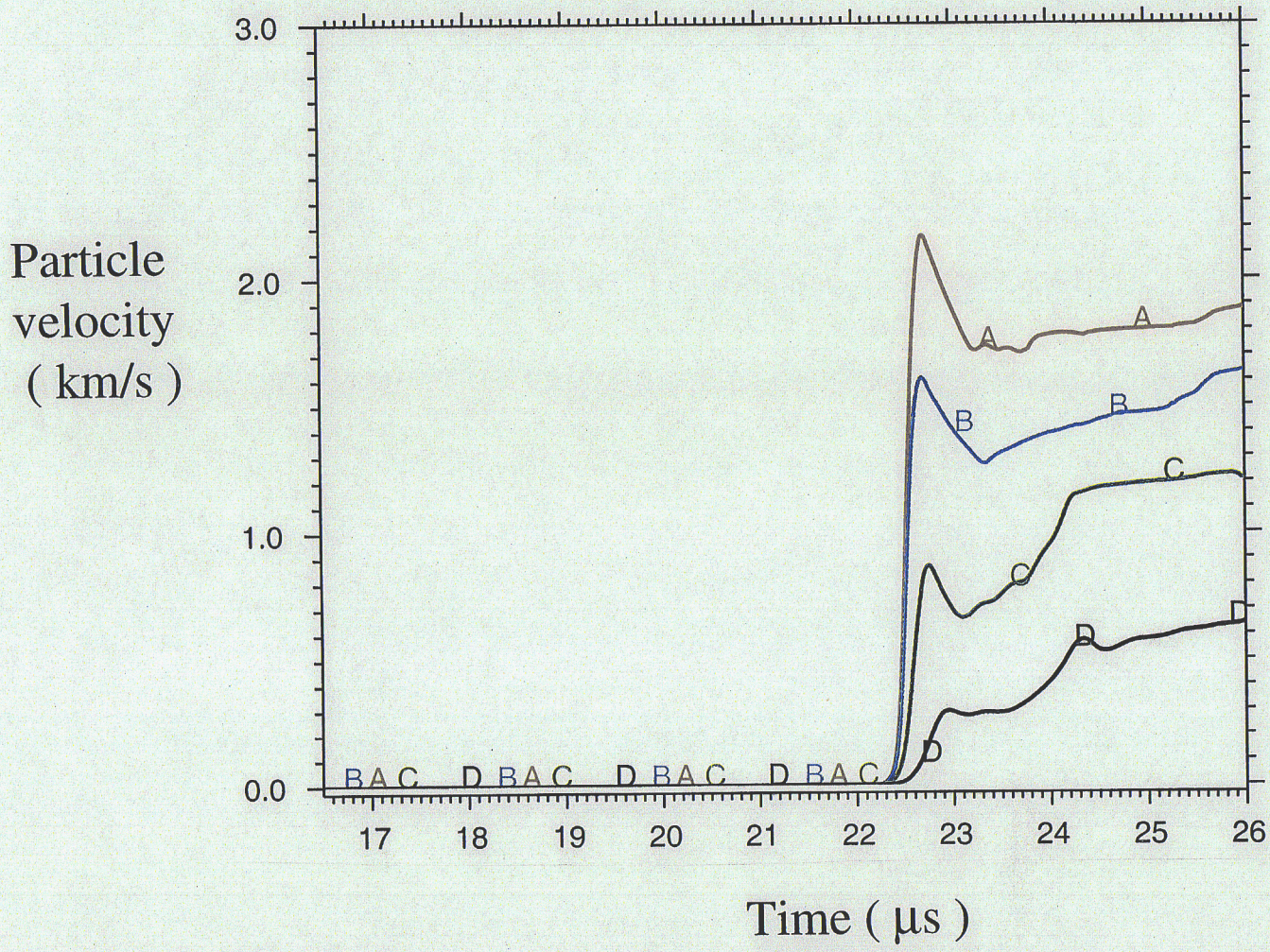

Figure 18

clpb--2-mg-7-11-2001

First series CLP EOS experiments modeling calculations

12.7mm dia. proj. at 11km/s 100mm gap: t=12μs mat. plot and zoning

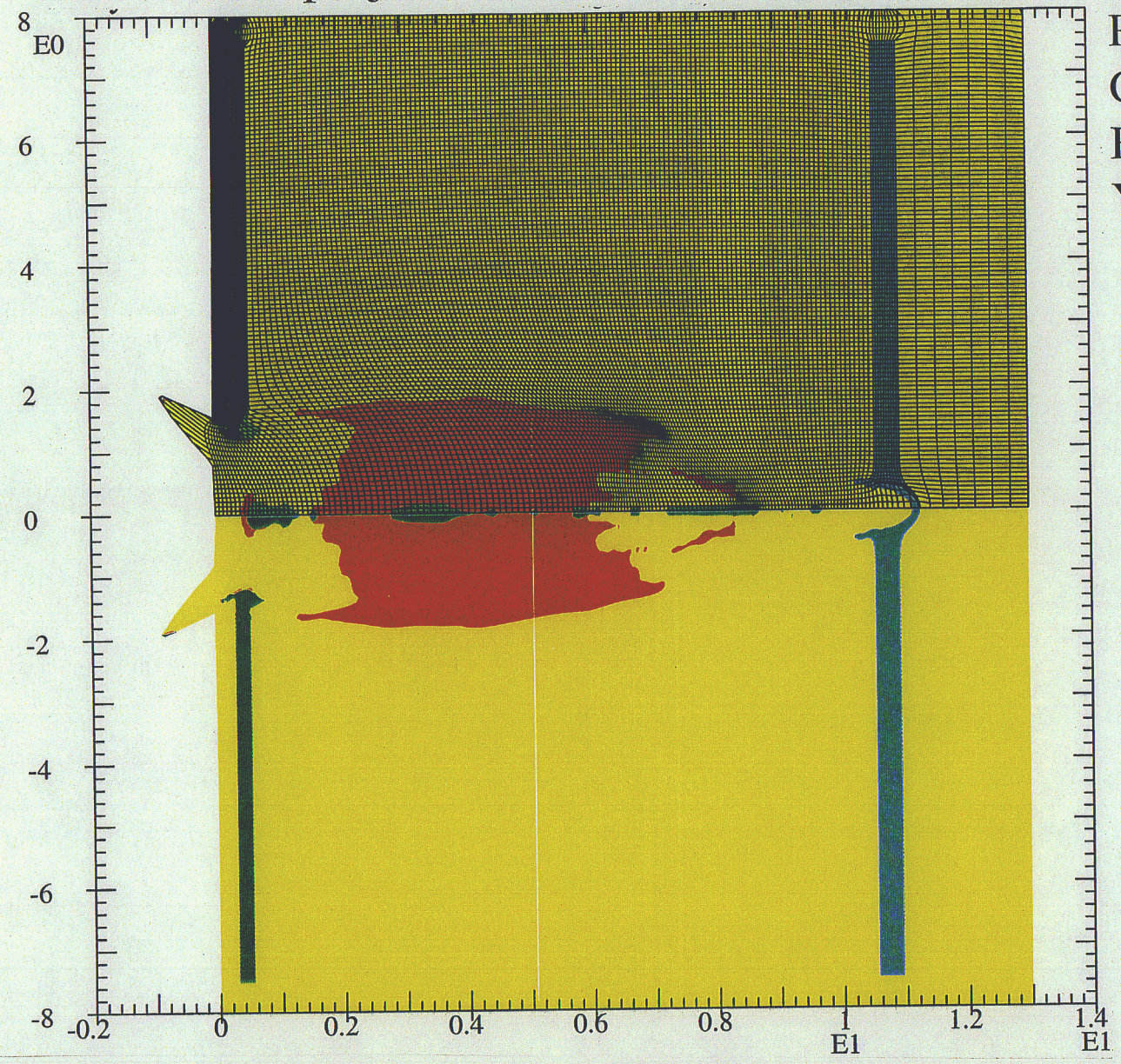

Red: projectile
Green: target
Blue: witness plate
Yellow: vacuum background

clpb--13-mg-7-12-2001

Figure 19

First series CLP EOS experiments modeling calculations

12.7mm diameter projectile at 11km/s 100mm gap: particle velocities at rear of witness plate on axis and 2,4 and 6mm away

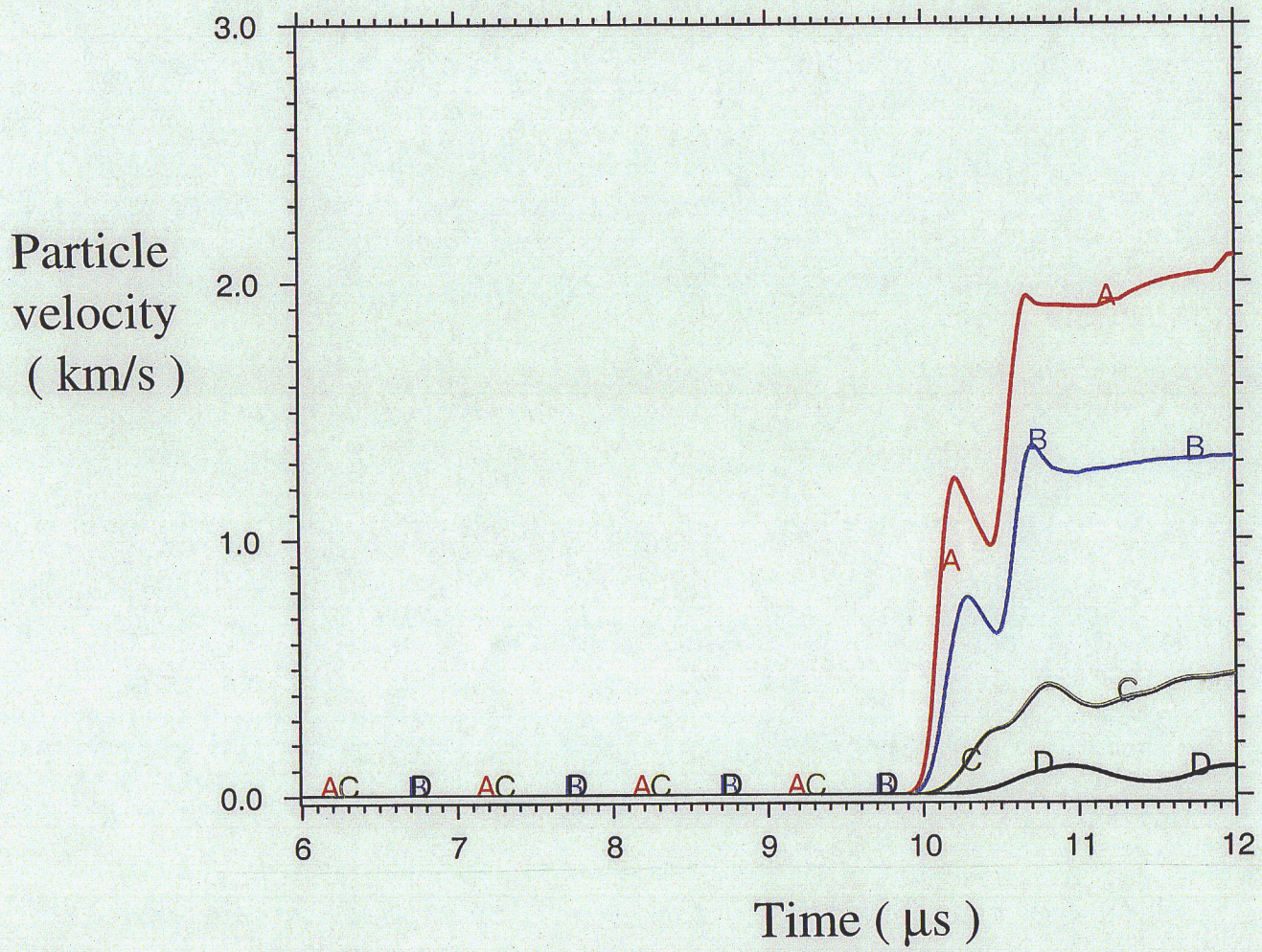

Figure 20

clpb--3-mg-7-11-2001

First series CLP EOS experiments modeling calculations

17mm dia. proj. at 11km/s 100mm gap: t=12μs mat. plot and zoning

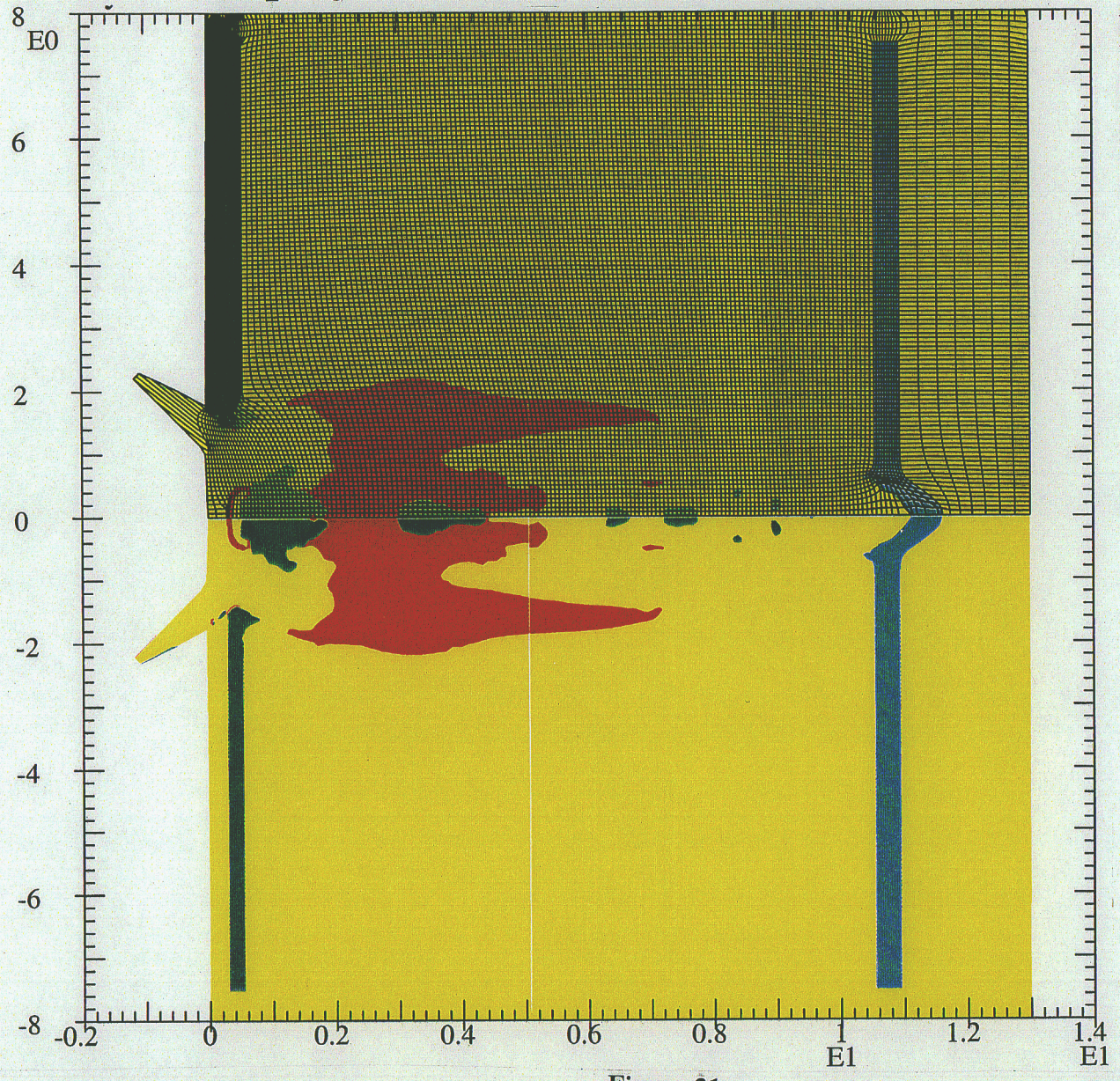

Red: projectile
Green: target
Blue: witness plate
Yellow: vacuum background

clpb--14-mg-7-12-2001

Figure 21

First series CLP EOS experiments modeling calculations

17mm diameter projectile at 11km/s 100mm gap: particle velocities at rear of witness plate on axis and 2,4 and 6mm away

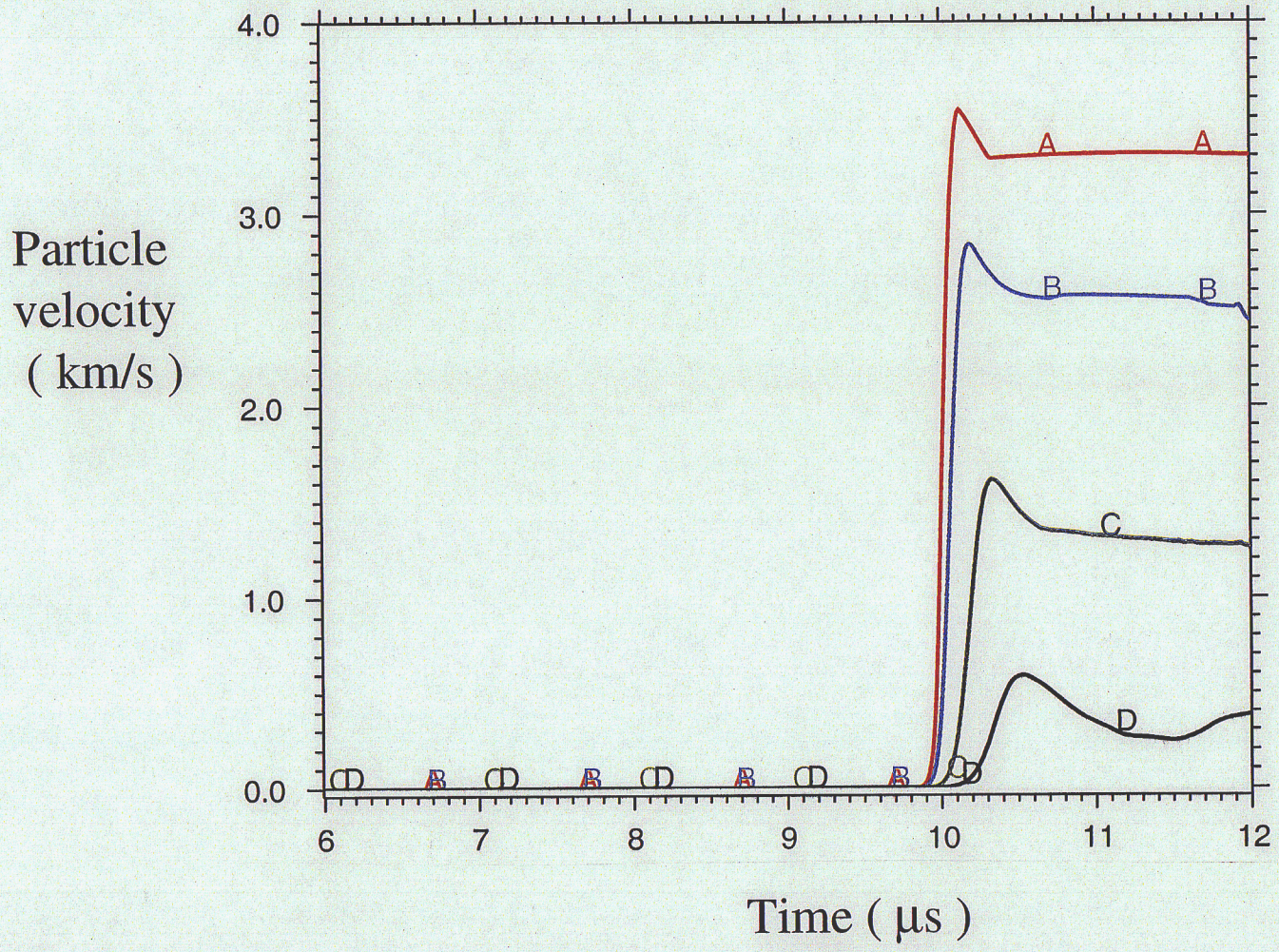

Figure 22

clpb--4-mg-7-11-2001

First series CLP EOS experiments modeling calculations

17mm dia. proj. at 6km/s 150mm gap: t=38μs mat. plot and zoning

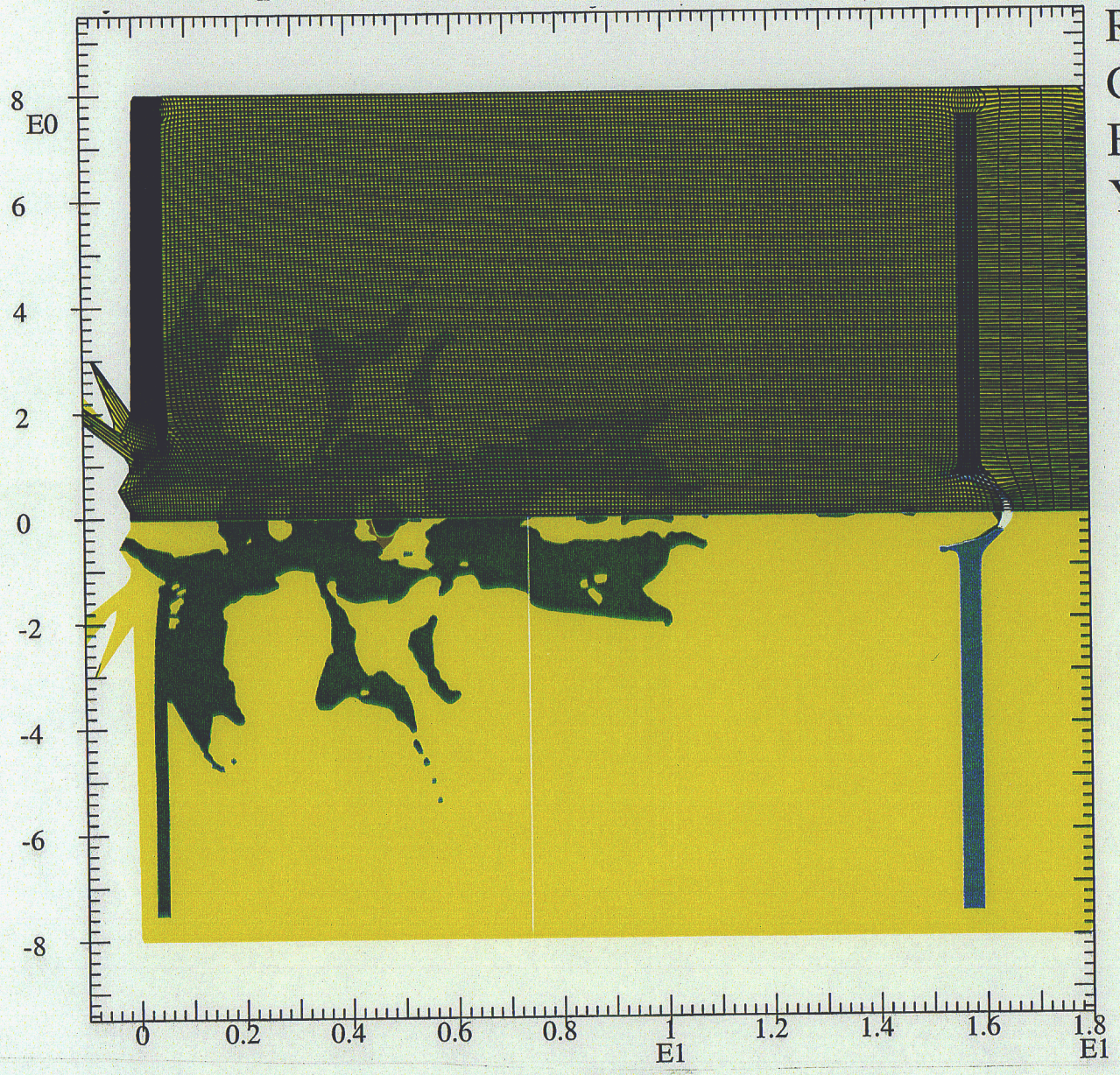

Red: projectile
Green: target
Blue: witness plate
Yellow: vacuum background

clpb--15-mg-7-12-2001

Figure 23

First series CLP EOS experiments modeling calculations

17mm diameter projectile at 6km/s 150mm gap: particle velocities at rear of witness plate on axis and 2,4 and 6mm away

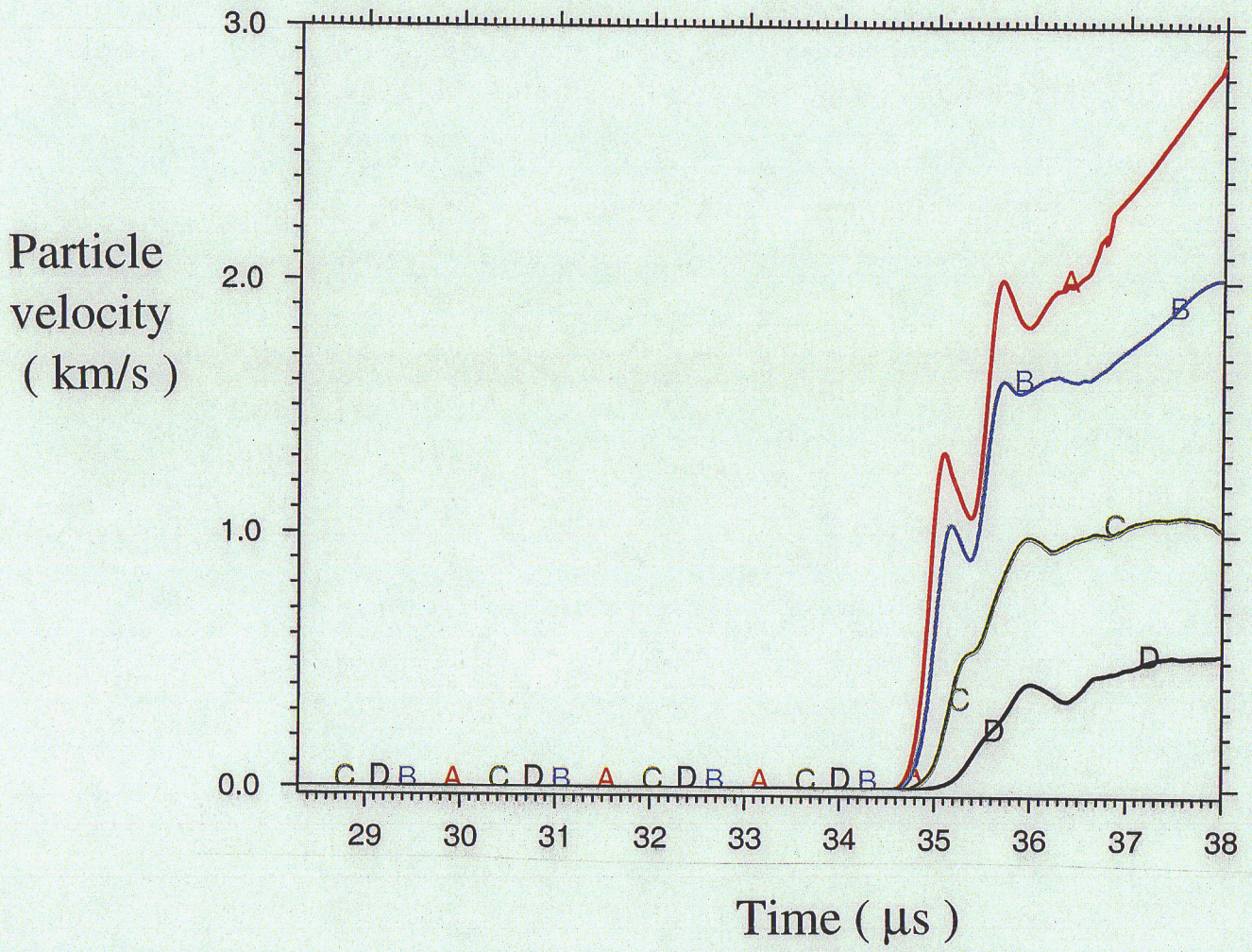

Figure 24

clpb--5-mg-7-11-2001

First series CLP EOS experiments modeling calculations

17mm dia. proj. at 11km/s 150mm gap: t=18μs mat. plot and zoning

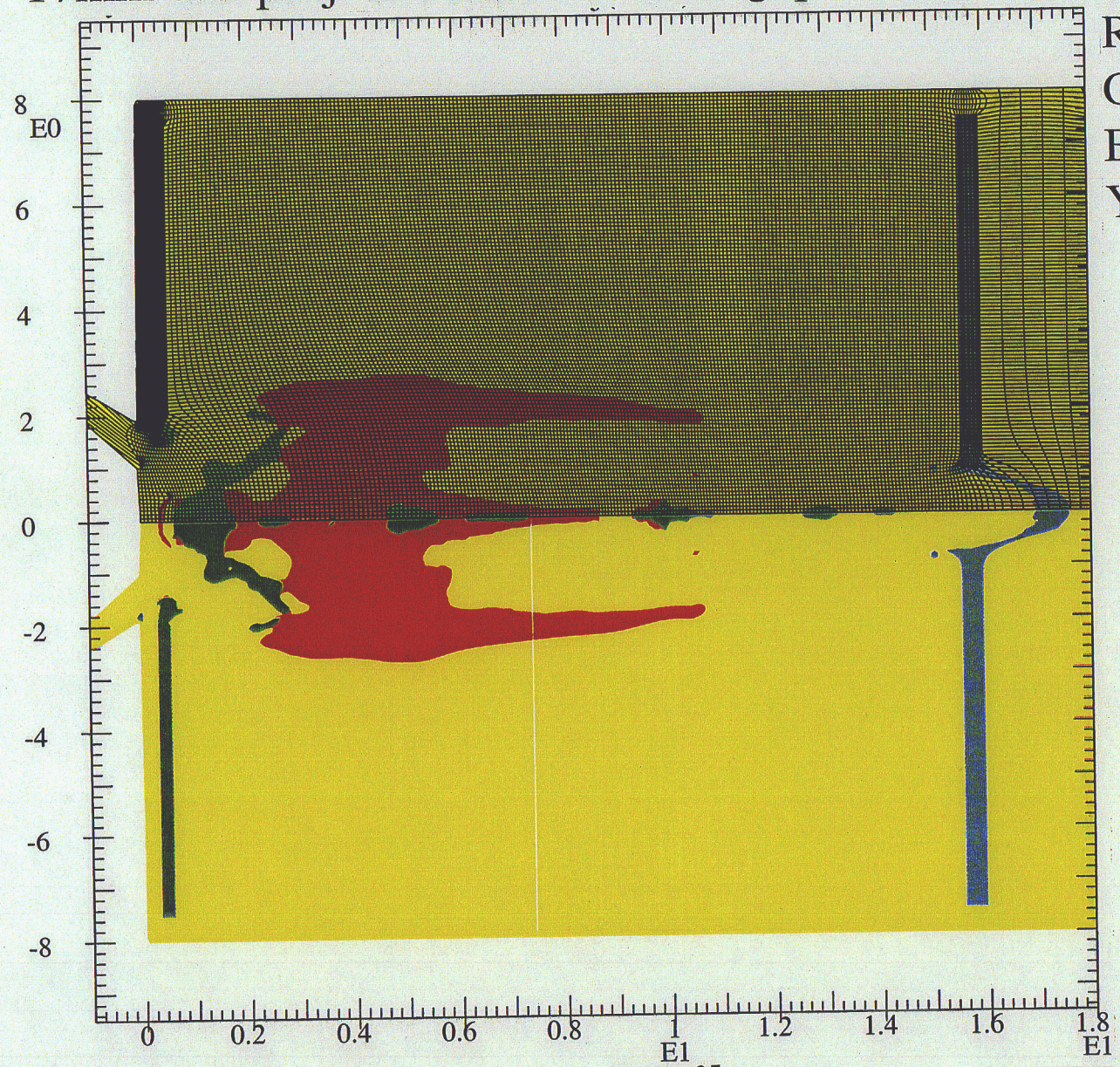

Red: projectile
Green: target
Blue: witness plate
Yellow: vacuum background

clpb--16-mg-7-12-2001

Figure 25

First series CLP EOS experiments modeling calculations

17mm diameter projectile at 11km/s 150mm gap: particle velocities at rear of witness plate on axis and 2,4 and 6mm away

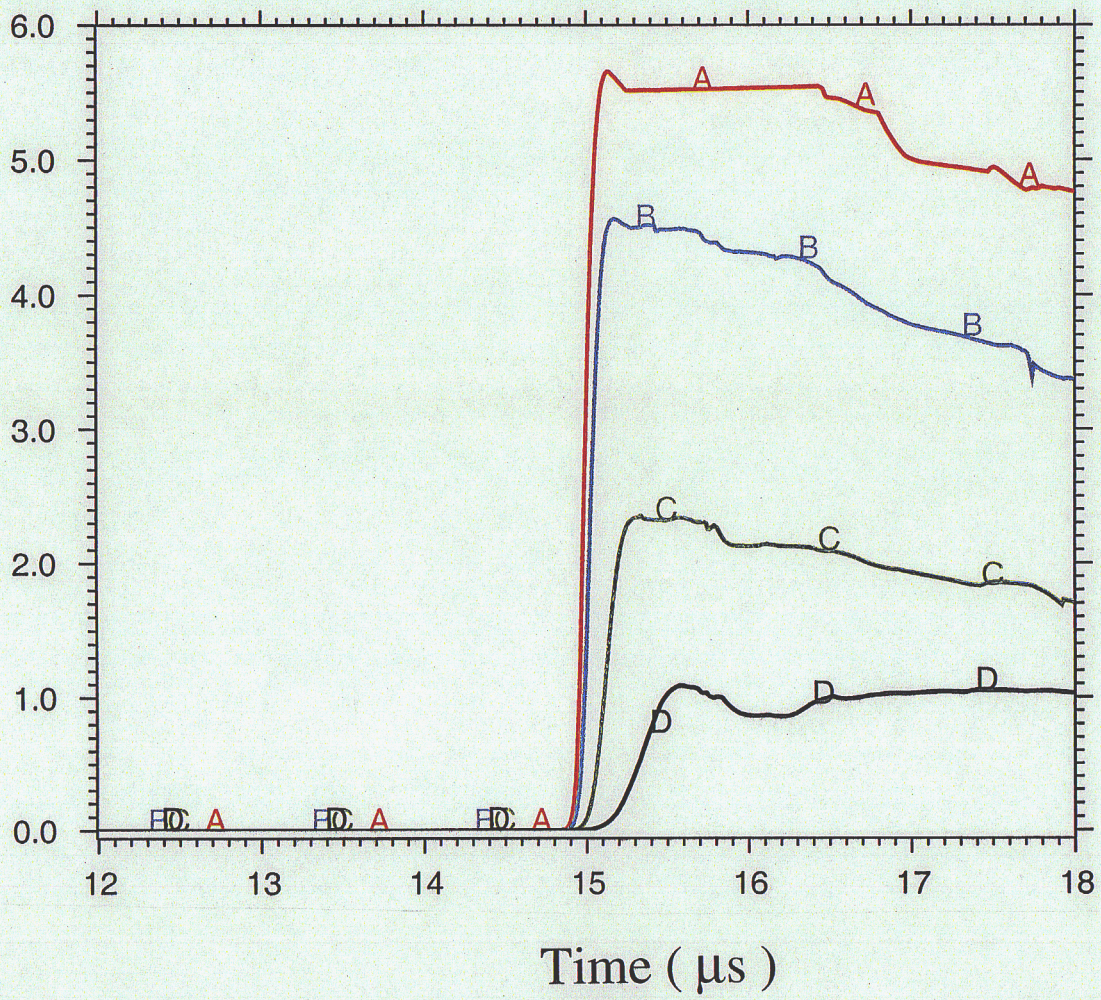

Figure 26

clpb--6-mg-7-11-2001

First series CLP EOS experiments modeling calculations particle velocity profile gap dependence

12.7mm diameter projectile at 6km/s particle velocity at rear of witness plate on axis and 2,4 and 6mm away, 75 and 100mm gaps

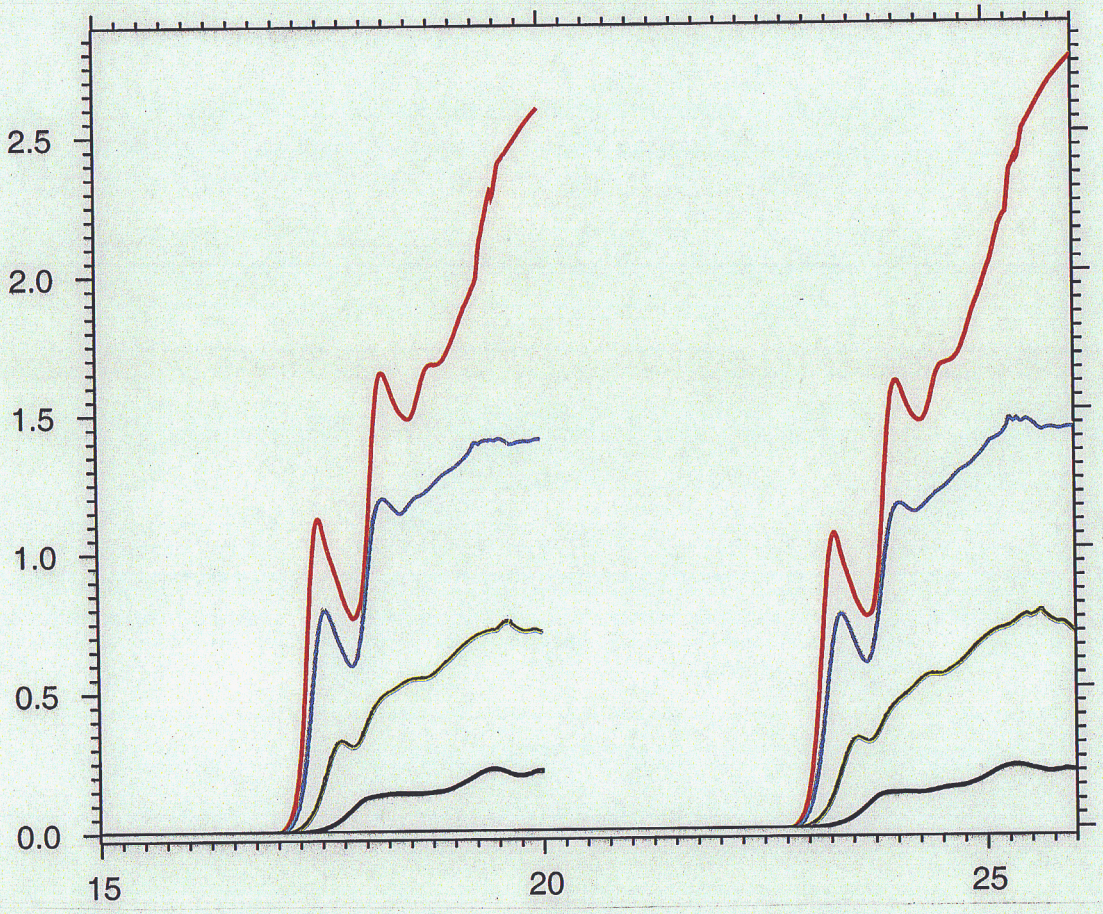

clpb--7-mg-7-11-2001

Figure 27

First series CLP EOS experiments modeling calculations particle velocity profile gap dependence

12.7mm diameter projectile at 11km/s particle velocity at rear of witness plate on axis and 2,4 and 6mm away, 75 and 100mm gaps

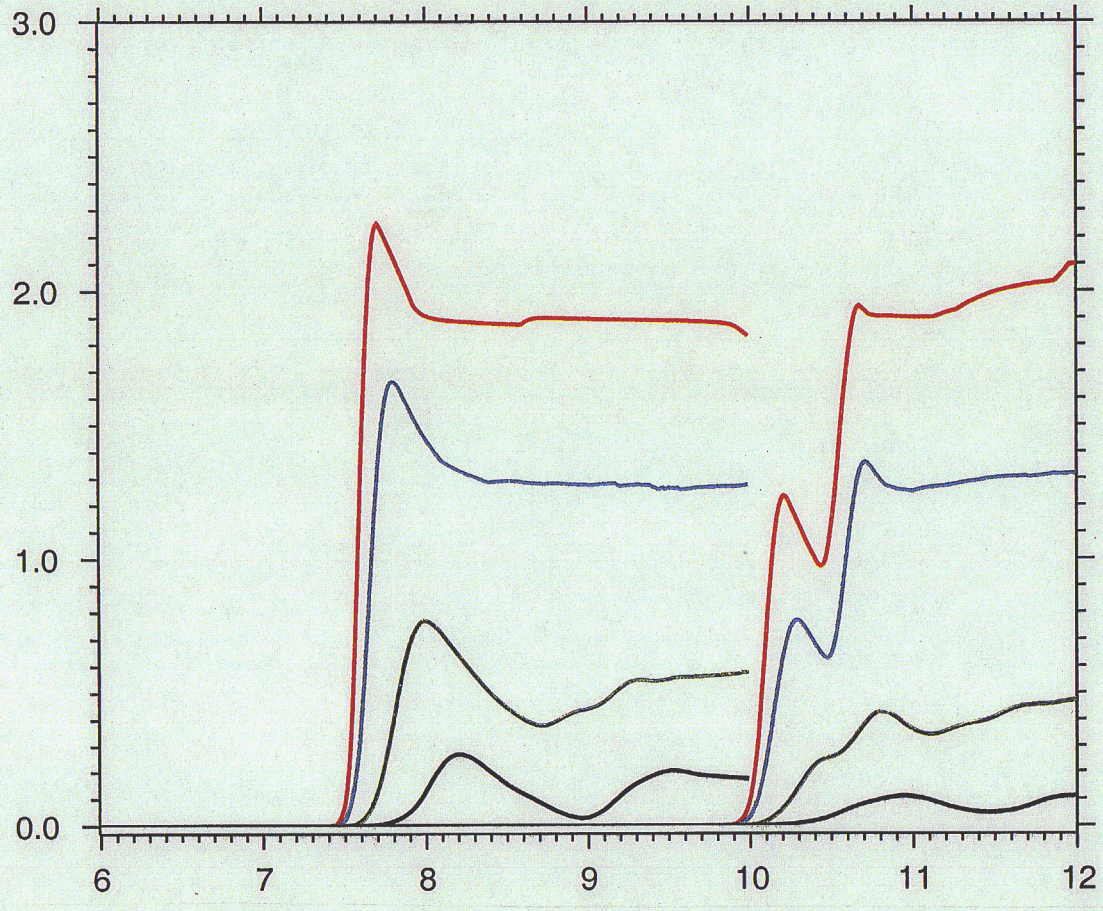

clpb--8-mg-7-11-2001

Figure 28

First series CLP EOS experiments modeling calculations particle velocity profile gap dependence

17mm diameter projectile at 6km/s particle velocity at rear of witness plate on axis and 2,4 and 6mm away 75,100 and 150mm gaps

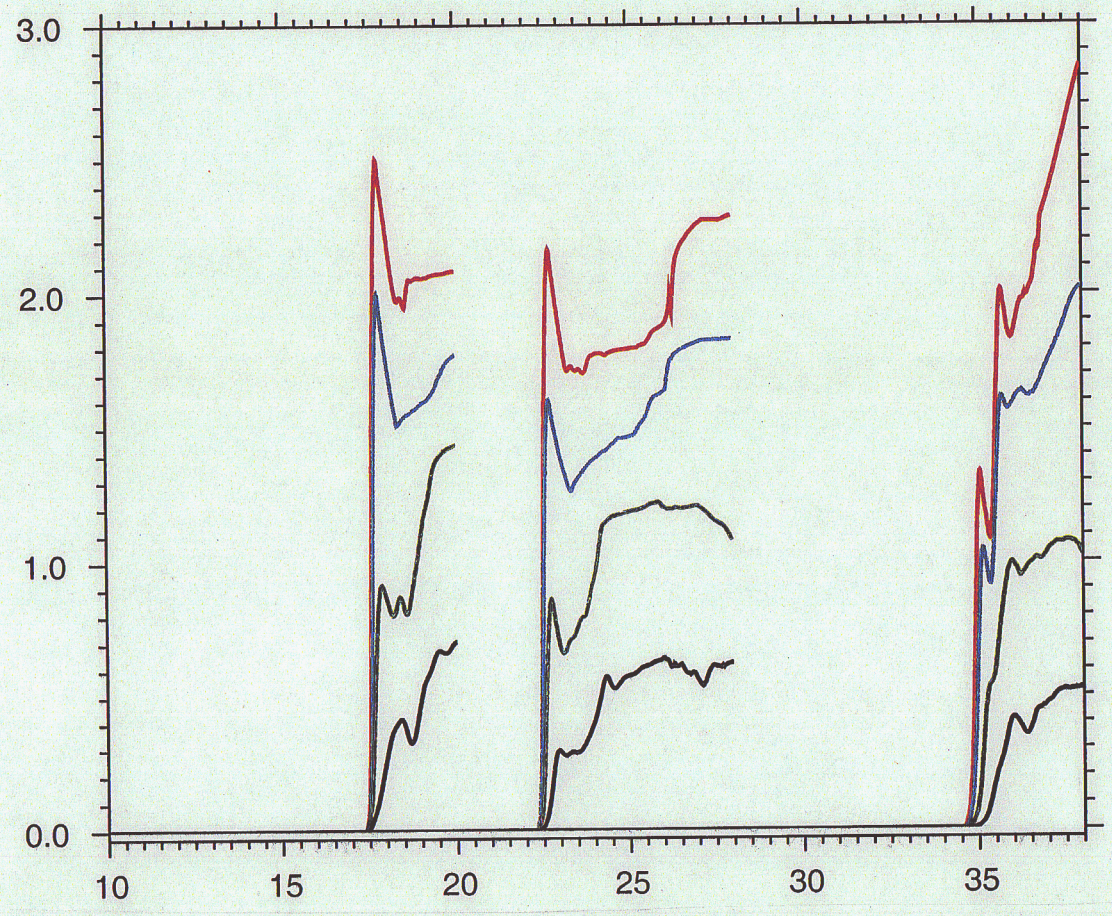

clpb--9-mg-7-11-2001

Figure 29

First series CLP EOS experiments modeling calculations particle velocity profile gap dependence

17mm diameter projectile at 11km/s particle velocity at rear of witness plate on axis and 2,4 and 6mm away 75,100 and 150mm gaps

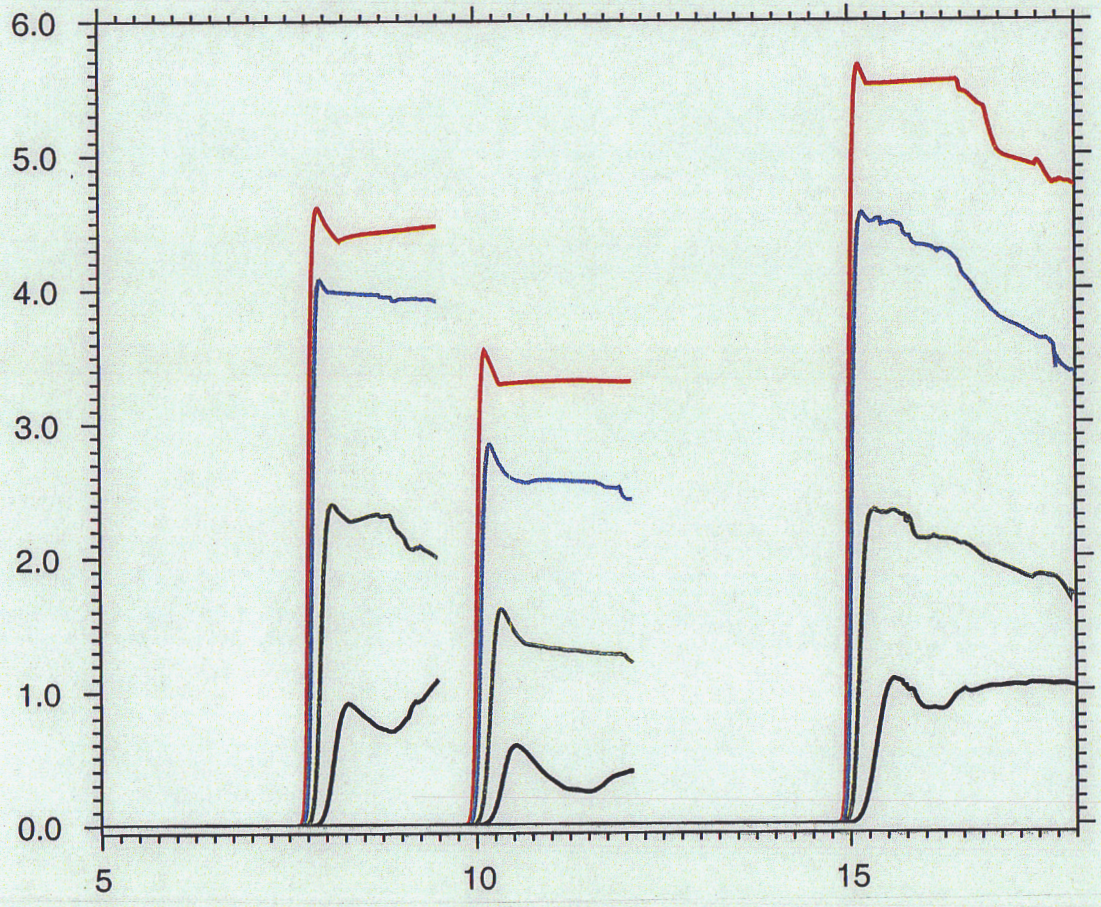

clpb--10-mg-7-11-2001

Figure 30

Second series CLP EOS experiments modeling calculations

Standard zoning (150x113) 17mm diameter projectile materials plot

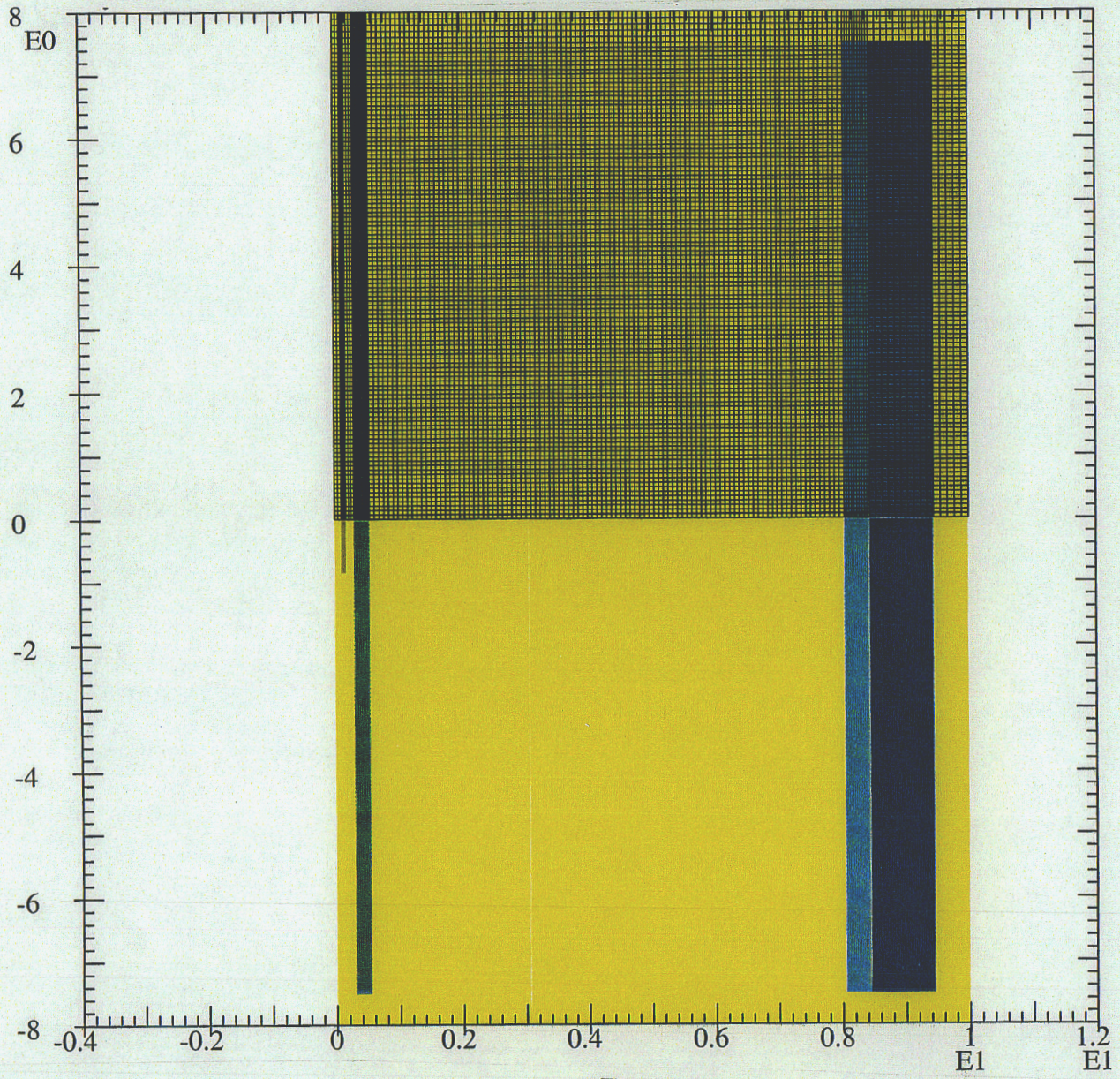

Red: projectile
Green: target
Blue: witness plate
Dark blue: LiF
Yellow: vacuum background

clpa--14-mg-6-19-2001

Figure 31

Second series CLP EOS experiments modeling calculations

Standard zoning (150x113) 17mm diameter projectile closeup

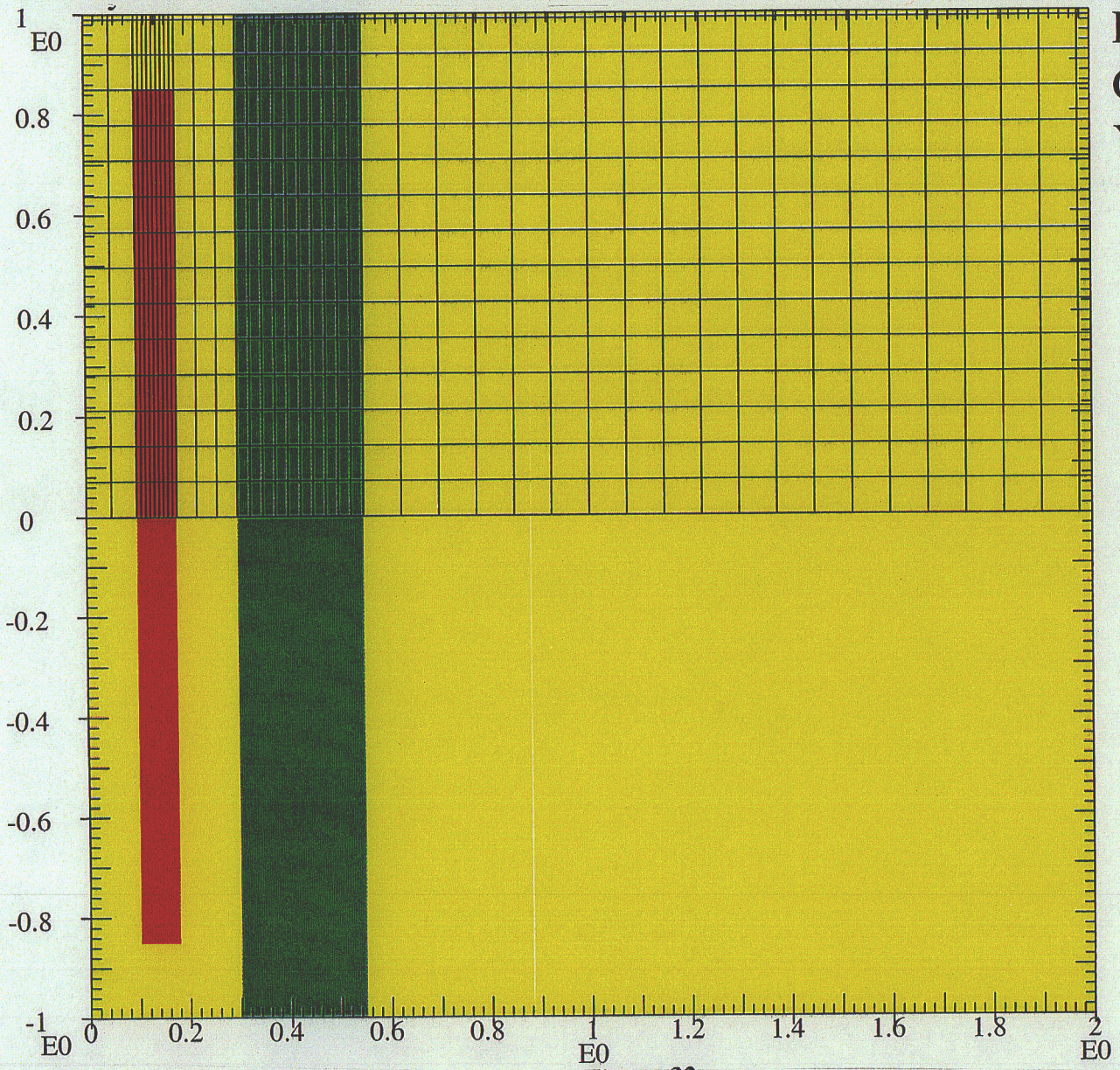

Red: projectile
Green: target
Yellow: vacuum background

clpa--15-mg-6-19-2001

Figure 32

Second series CLP EOS experiments modeling calculations

Standard zoning (150x113) closeup of witness plate and backing

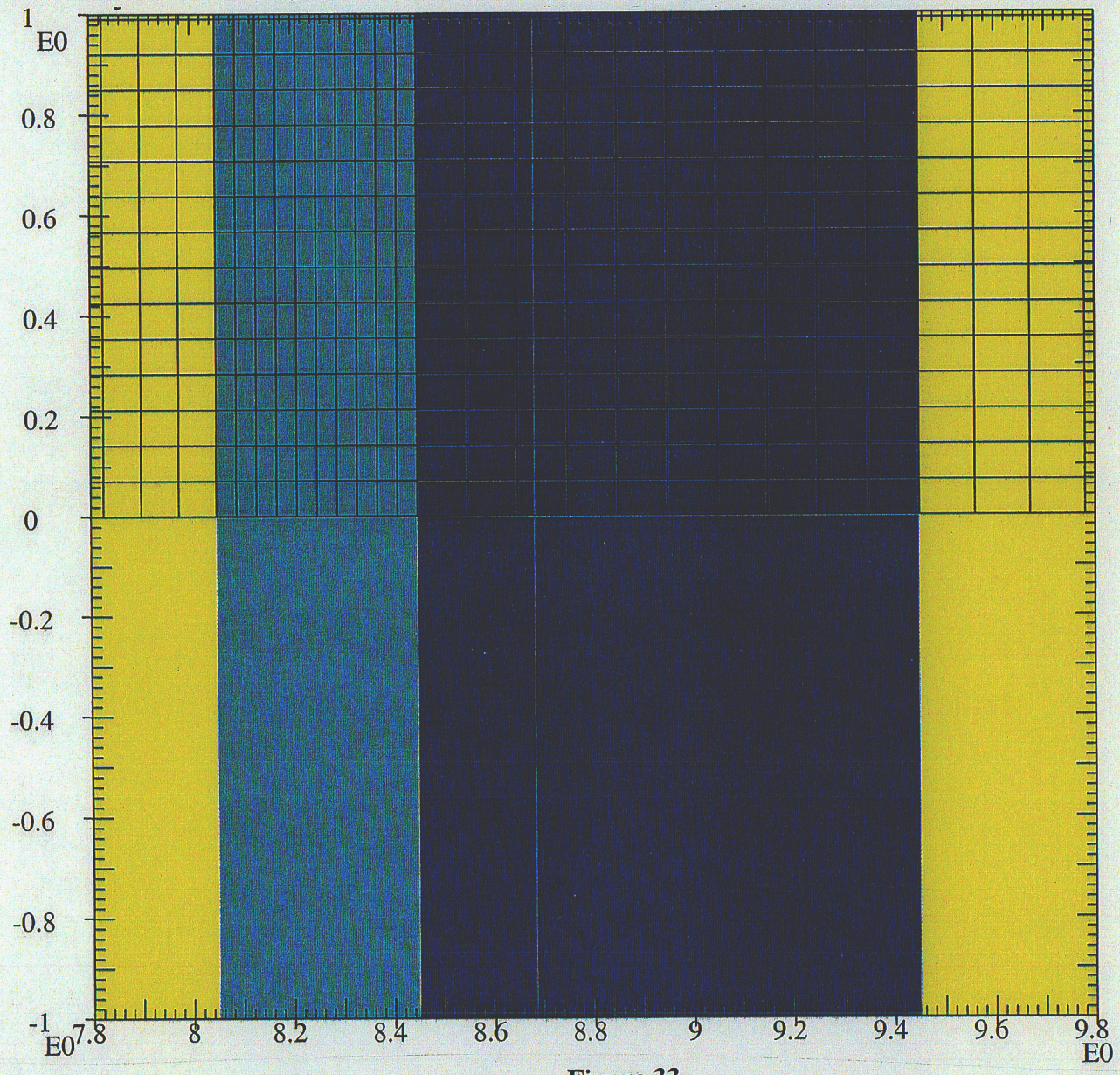

Blue: witness plate
Dark blue: LiF
Yellow: vacuum background

clpa--16-mg-6-21-2001

Figure 33

Second series CLP EOS experiments modeling calculations

Standard zoning (150x113) 17mm dia. proj. at 6km/s: t=20μs

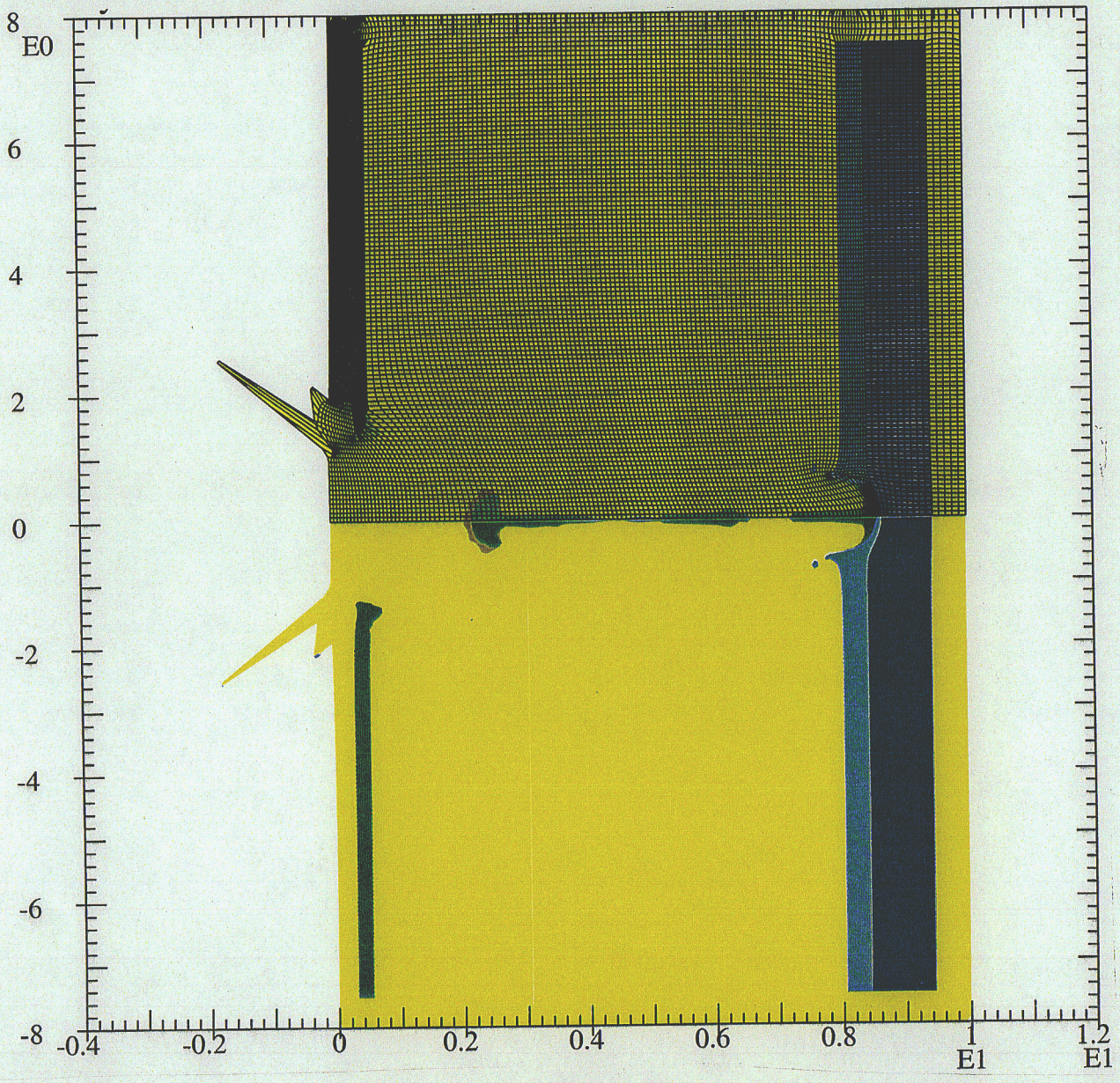

Red: projectile
Green: target
Blue: witness plate
Dark blue: LiF
Yellow: vacuum background

clpa--17-mg-6-21-2001

Figure 34

Second series CLP EOS experiments modeling calculations

Standard zoning (150x113) 17mm diameter projectile at 6km/s

Particle velocities at rear of witness plate on axis and 2,4 and 6mm away

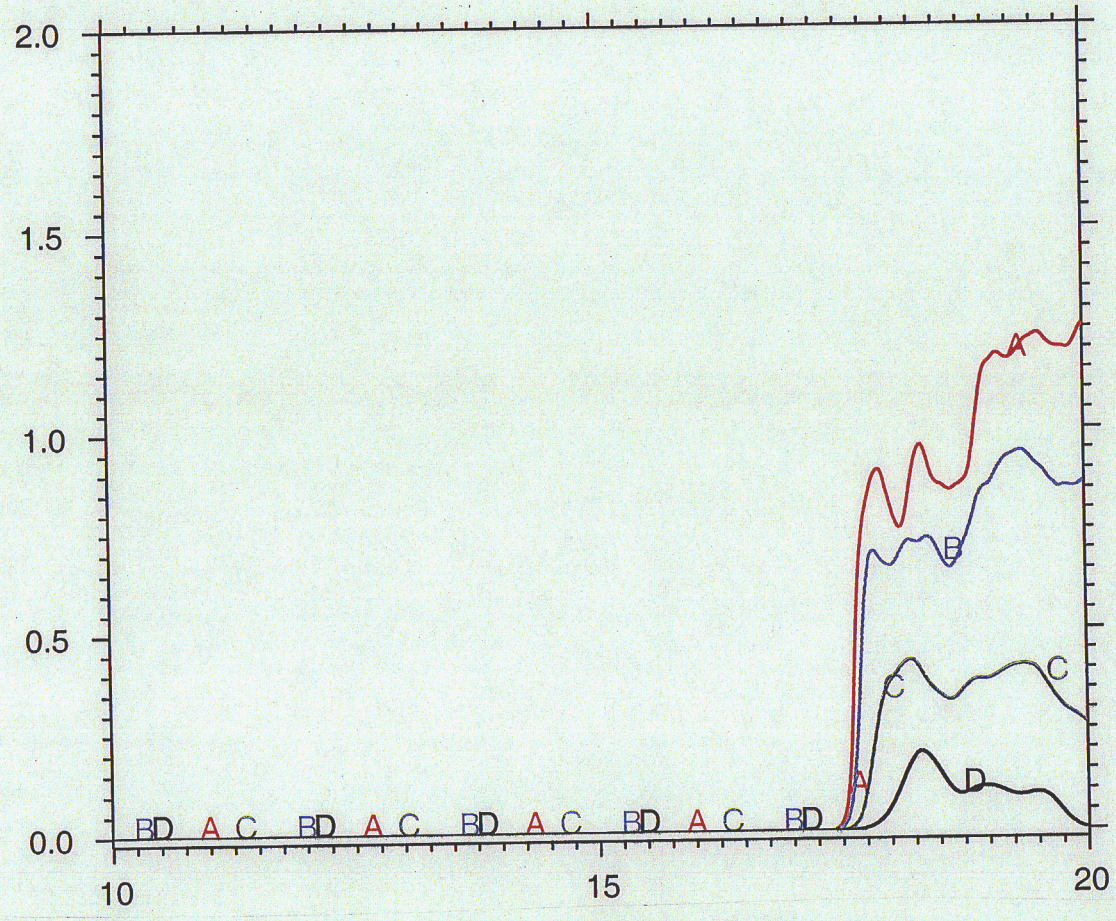

Particle velocity (km/s)

Time (μs)

Figure 35

clpa--18-mg-6-19-2001

Second series CLP EOS experiments modeling calculations

Standard zoning (150x113) 17mm dia. proj. at 11km/s: t=10μs

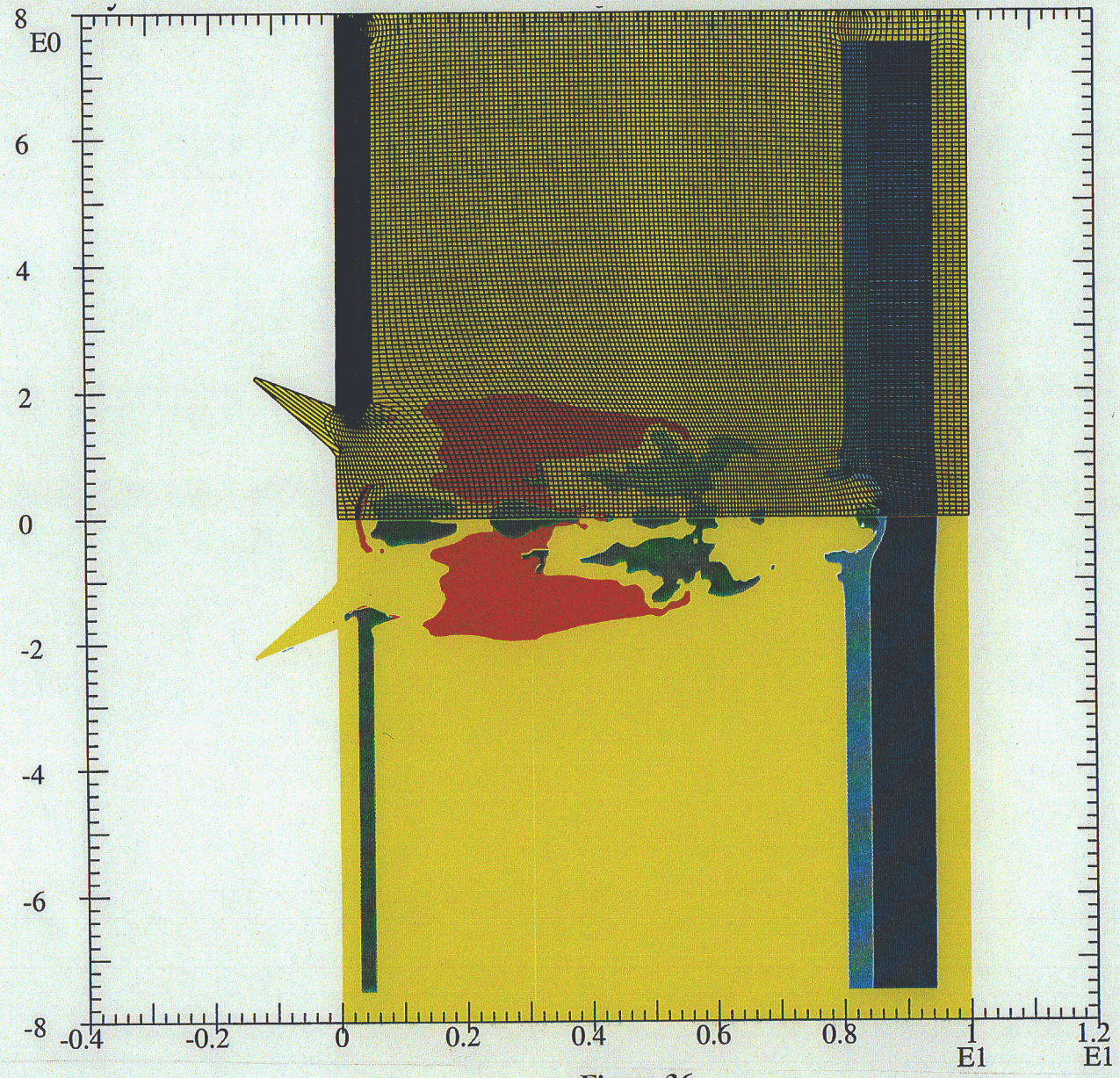

Red: projectile
Green: target
Blue: witness plate
Dark blue: LiF
Yellow: vacuum background

clpa--19-mg-6-21-2001

Figure 36

Second series CLP EOS experiments modeling calculations

Standard zoning (150x113) 17mm diameter projectile at 11km/s

Particle velocities at rear of witness plate on axis and 2,4 and 6mm away

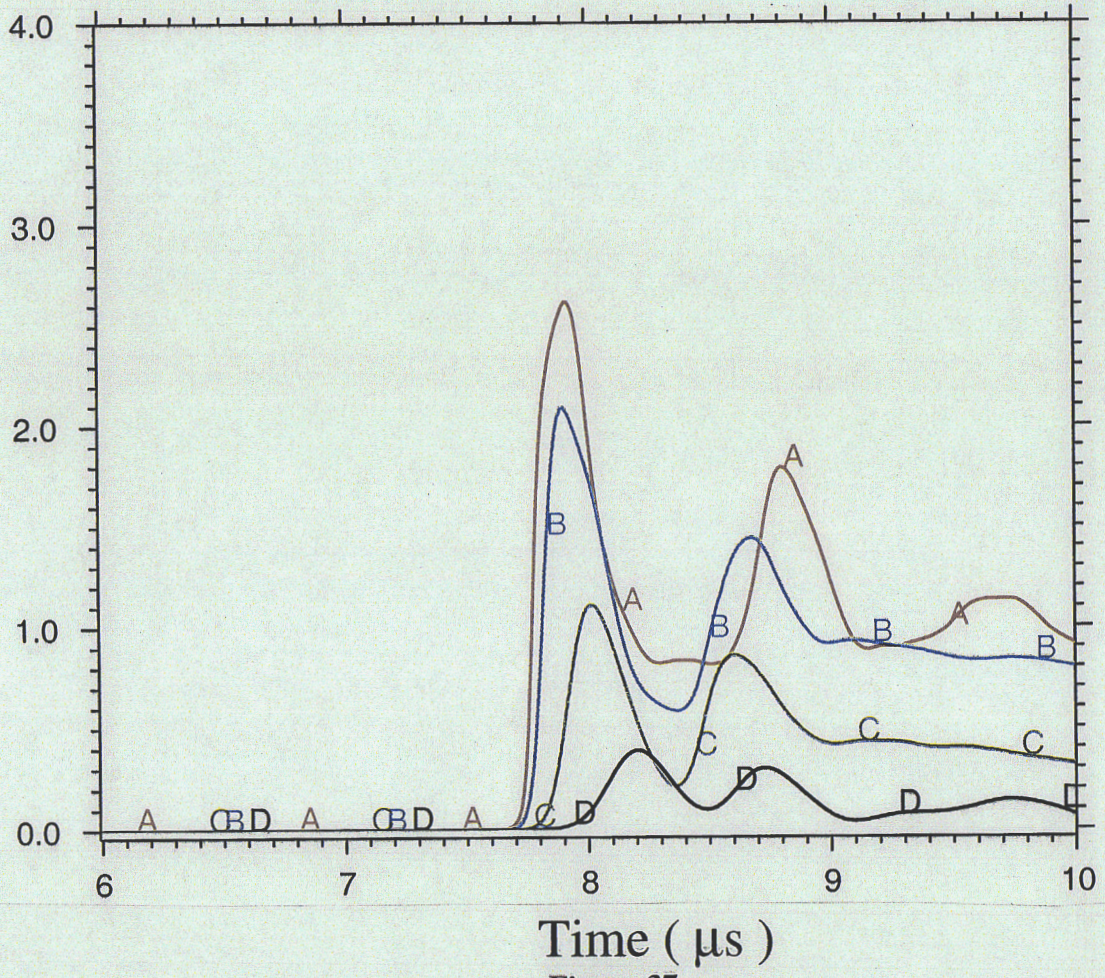

Figure 37

clpa--20-mg-6-19-2001

Second series CLP EOS experiments modeling calculations

Fine zoning (240x225) 17mmdia. proj. materials map and zoning at t=0

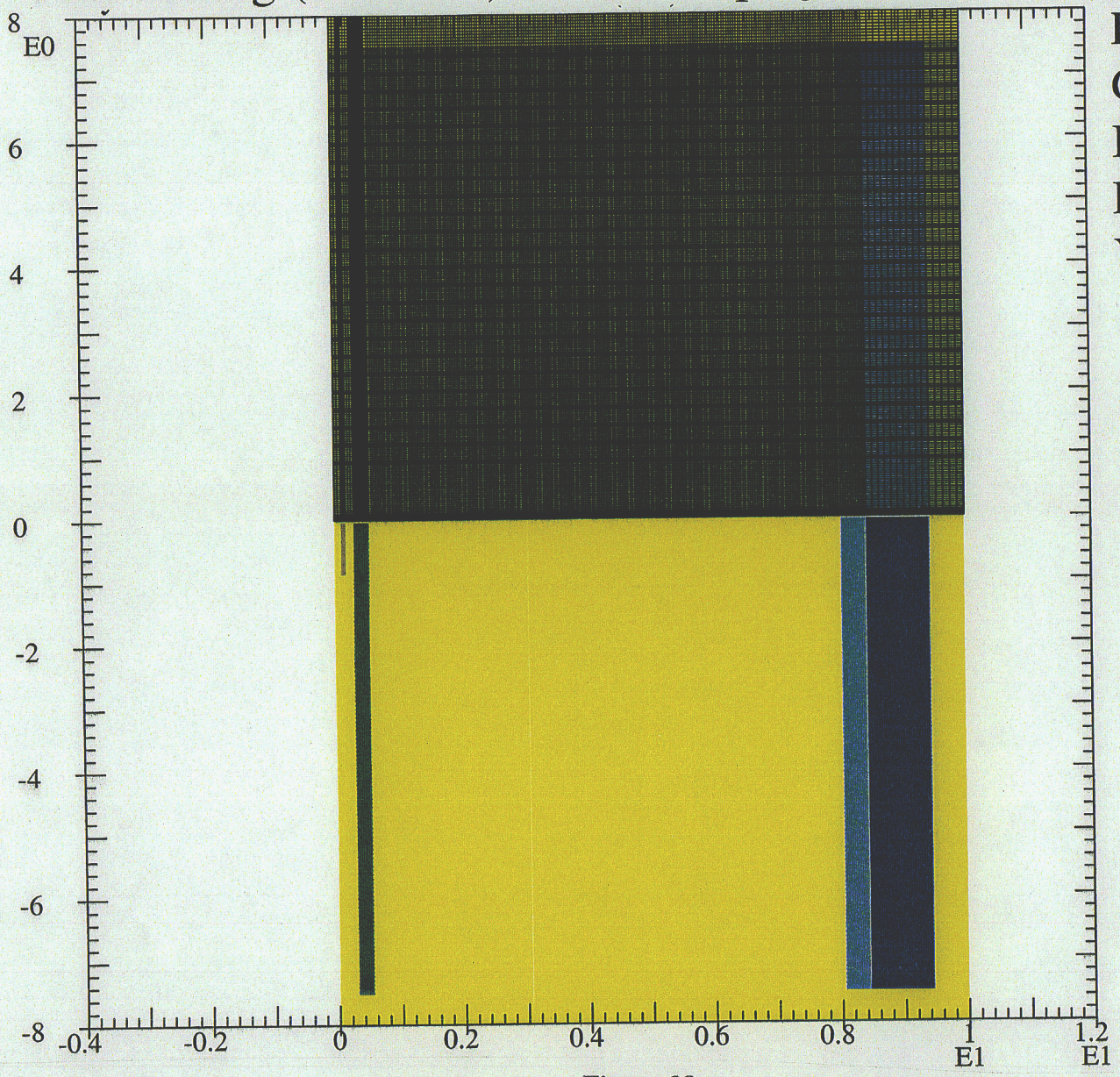

Red: projectile
Green: target
Blue: witness plate
Dark blue: LiF
Yellow: vacuum background

clpa--21-mg-6-19-2001

Figure 38

Second series CLP EOS experiments modeling calculations

Fine zoning (240x225) 17mm diameter projectile closeup at t=0

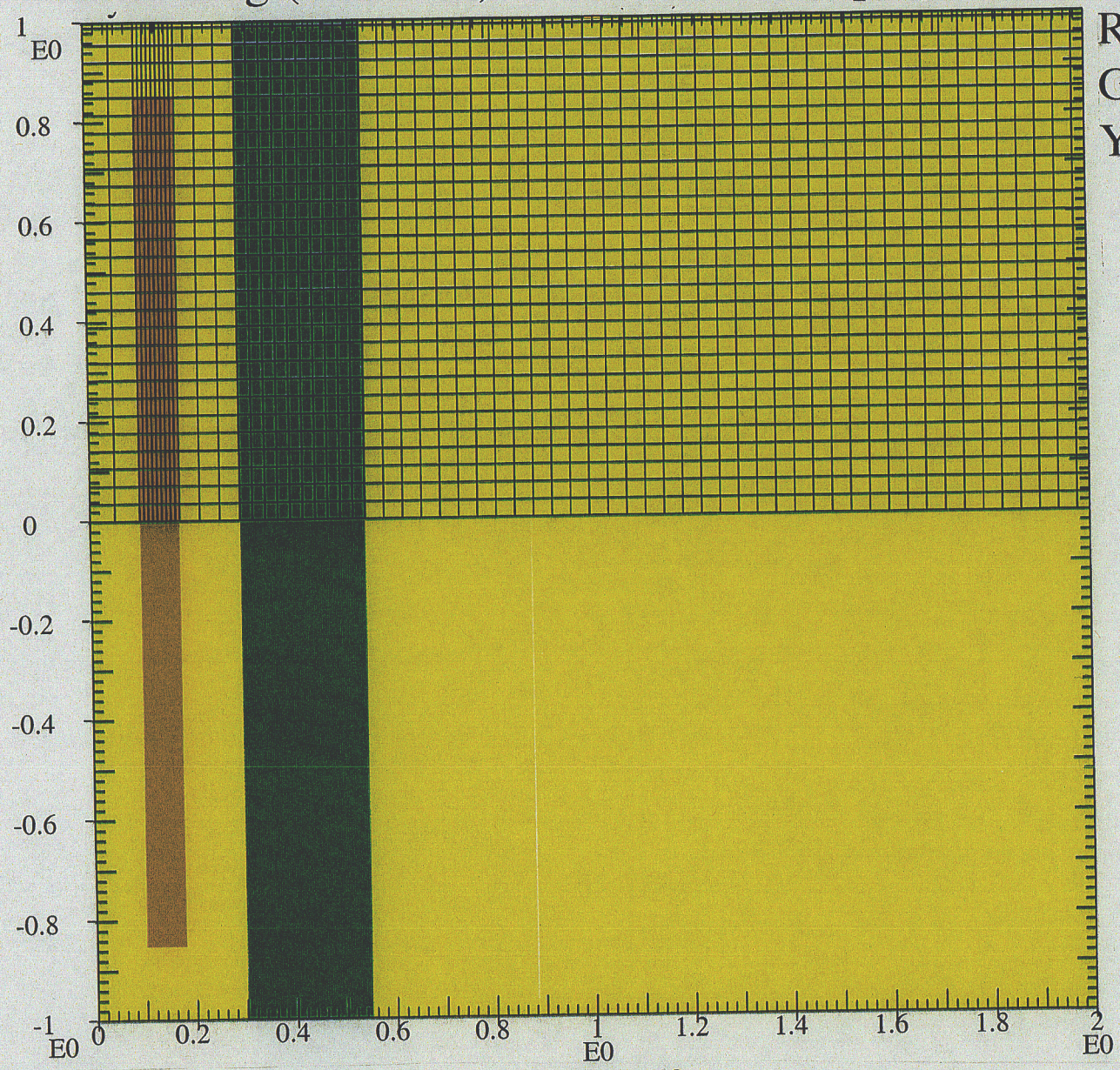

Red: projectile
Green: target
Yellow: vacuum background

clpa--22-mg-6-19-2001

Figure 39

Second series CLP EOS experiments modeling calculations

Fine zoning (240x225) witness plate and backing closeup at t=0

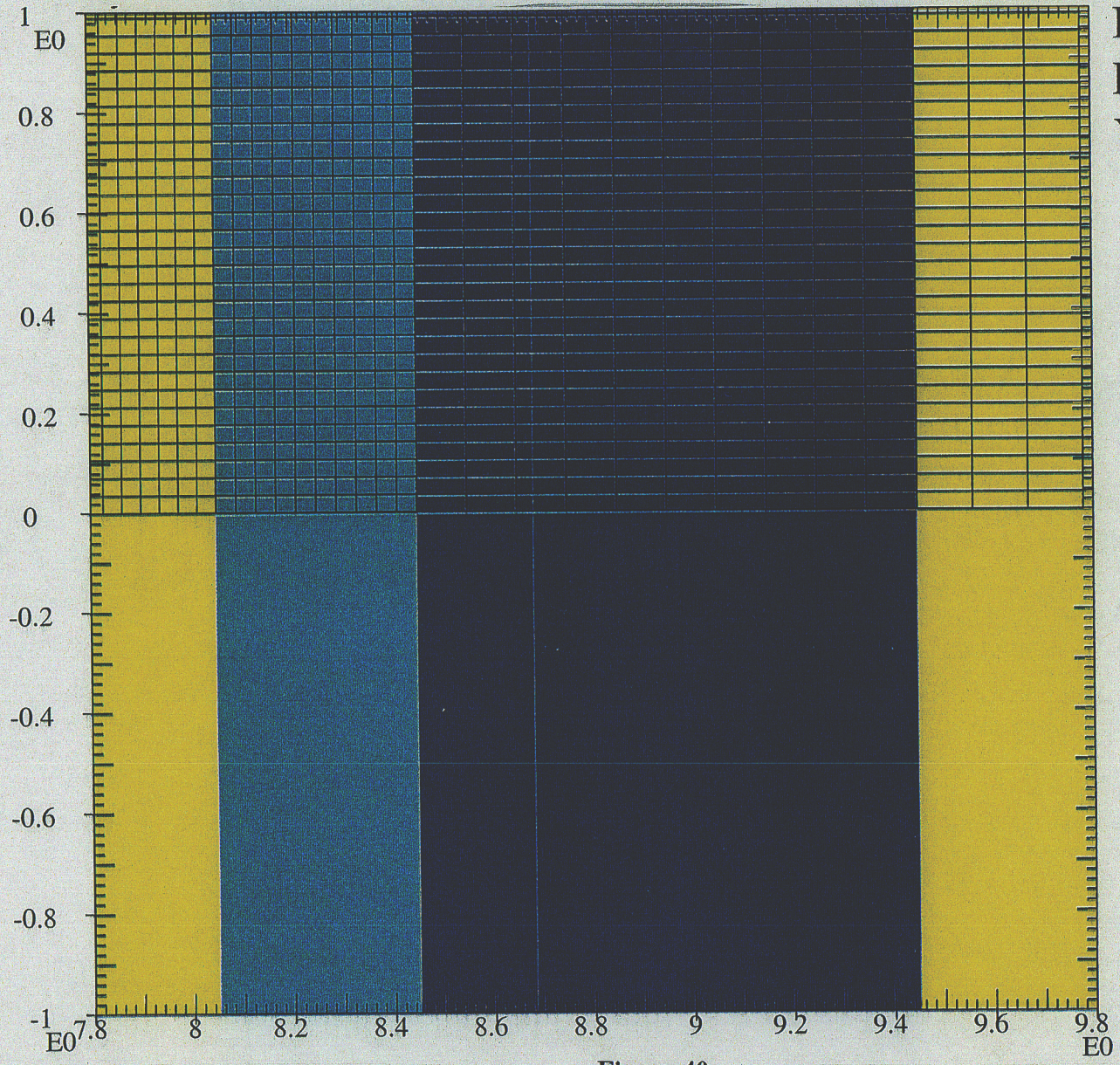

Blue: witness plate
Dark blue: LiF
Yellow: vacuum background

clpa--23-mg-6-19-2001

Figure 40

Second series CLP EOS experiments modeling calculations

Fine zoning (240x225) 17mm dia. proj. at 6km/s: t=20μs

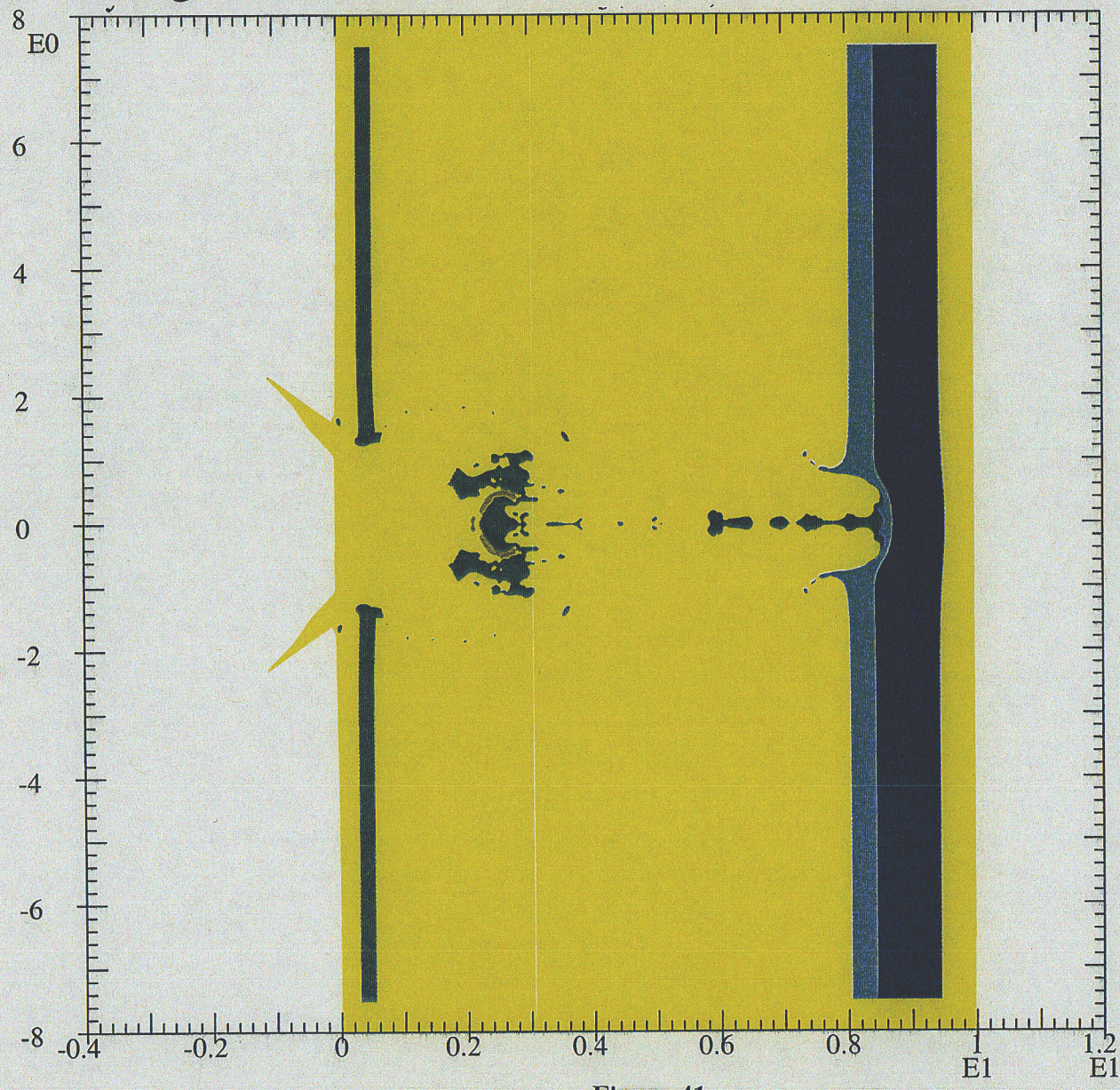

Red: projectile
Green: target
Blue: witness plate
Dark blue: LiF
Yellow: vacuum background

clpa--24-mg-6-21-2001

Figure 41

Second series CLP EOS experiments modeling calculations

Fine zoning (240x225) 17mm diameter projectile at 6km/s

Particle velocities at rear of witness plate on axis and 2,4 and 6mm away

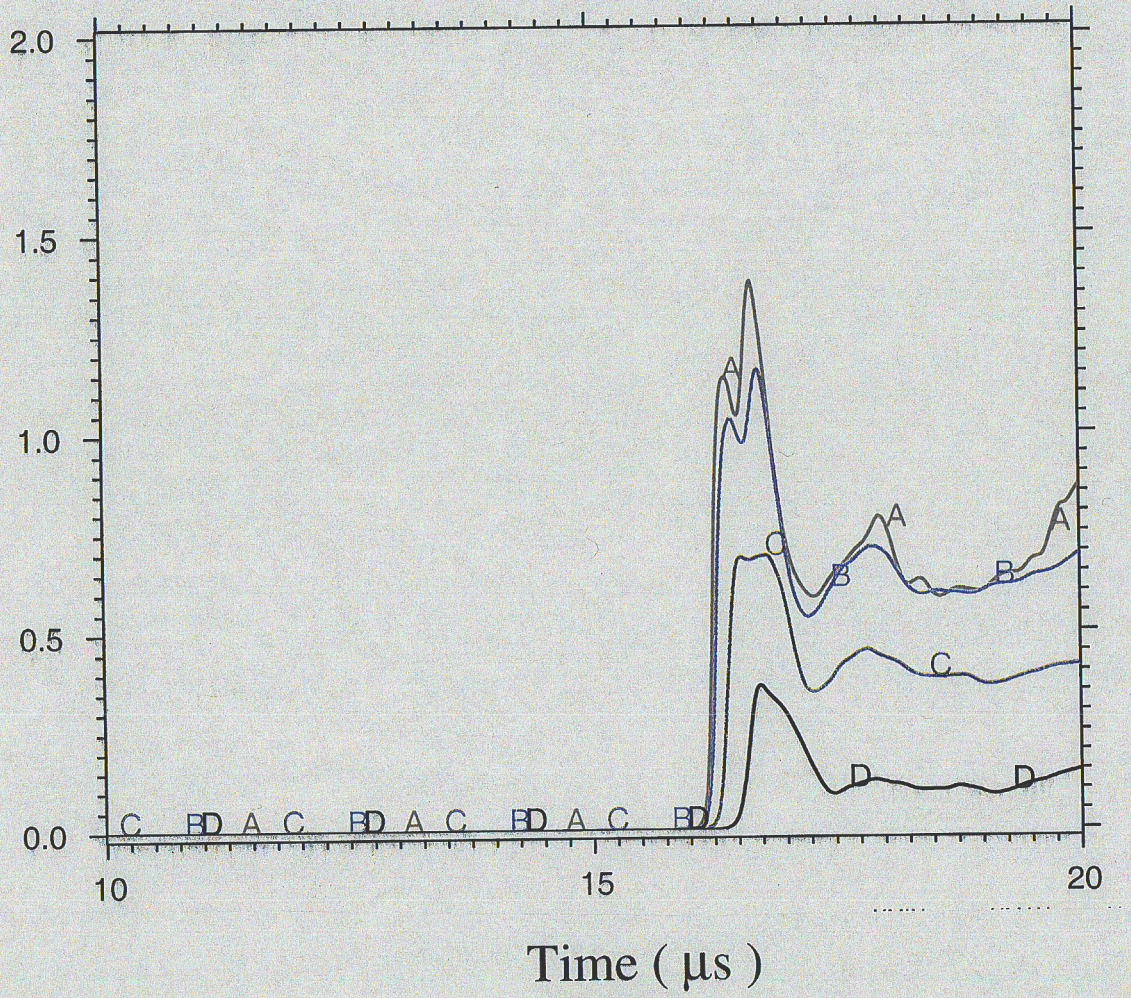

Particle velocity (km/s)

Time (μs)

Figure 42

clpa--25-mg-6-19-2001

Second series CLP EOS experiments modeling calculations

Fine zoning (240x225) 17mm dia. proj. at 11km/s: t=10μs

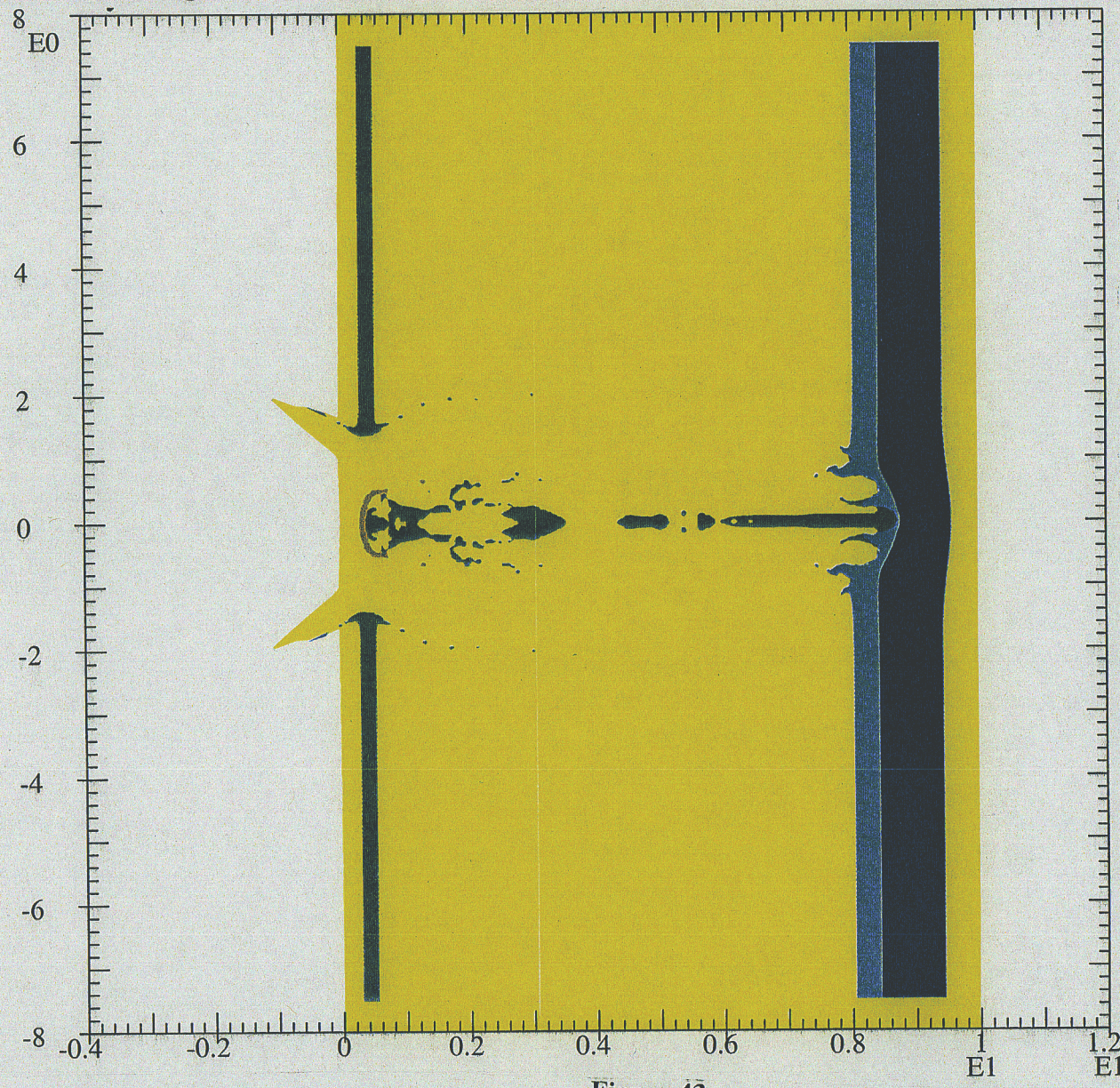

Red: projectile
Green: target
Blue: witness plate
Dark blue: LiF
Yellow: vacuum background

clpda--26-mg-6-21-2001

Figure 43

Second series CLP EOS experiments modeling calculations

Fine zoning (240x225) 17mm diameter projectile at 11km/s

Particle velocities at rear of witness plate on axis and 2,4 and 6mm away

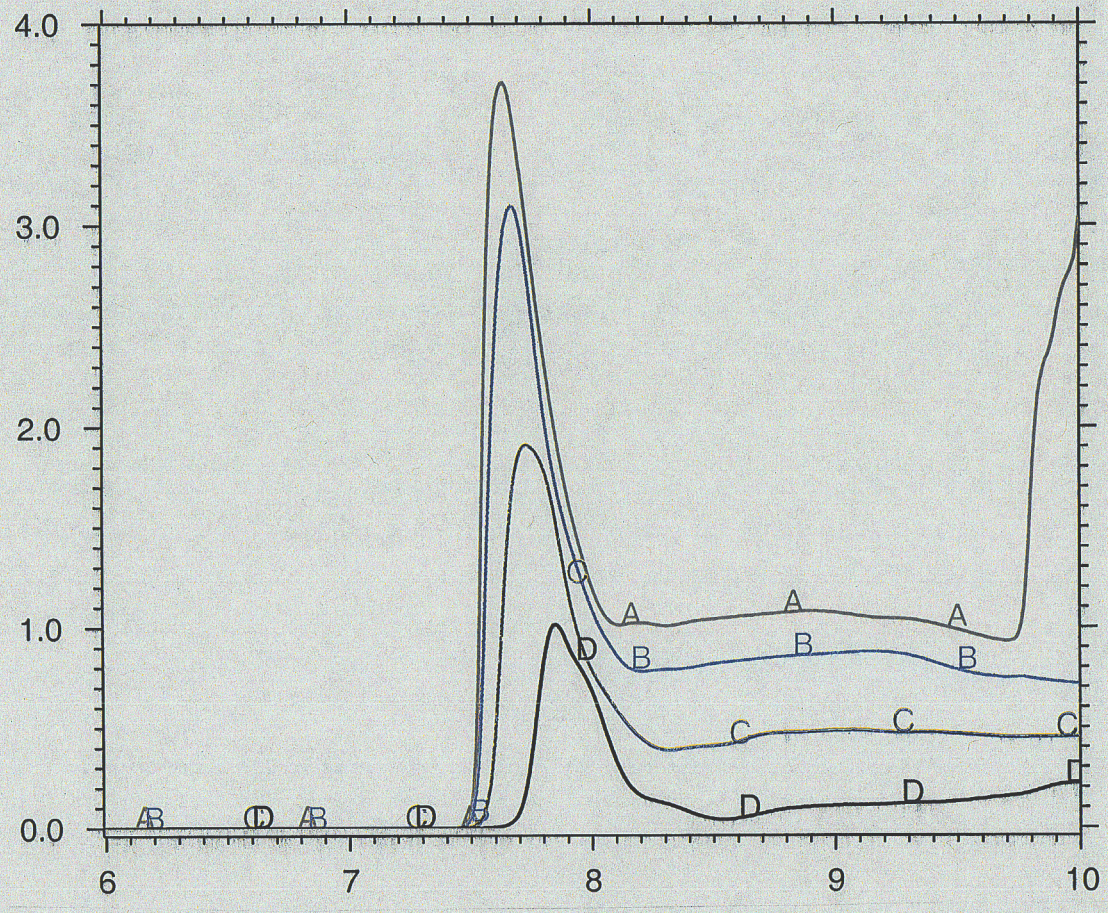

Particle velocity (km/s)

Time (μs)

Figure 44

clpa--27-mg-6-19-2001

Second series CLP EOS experiments modeling calculations

Very fine zoning (405x337) 17mm dia. proj. closeup and zoning at t=0

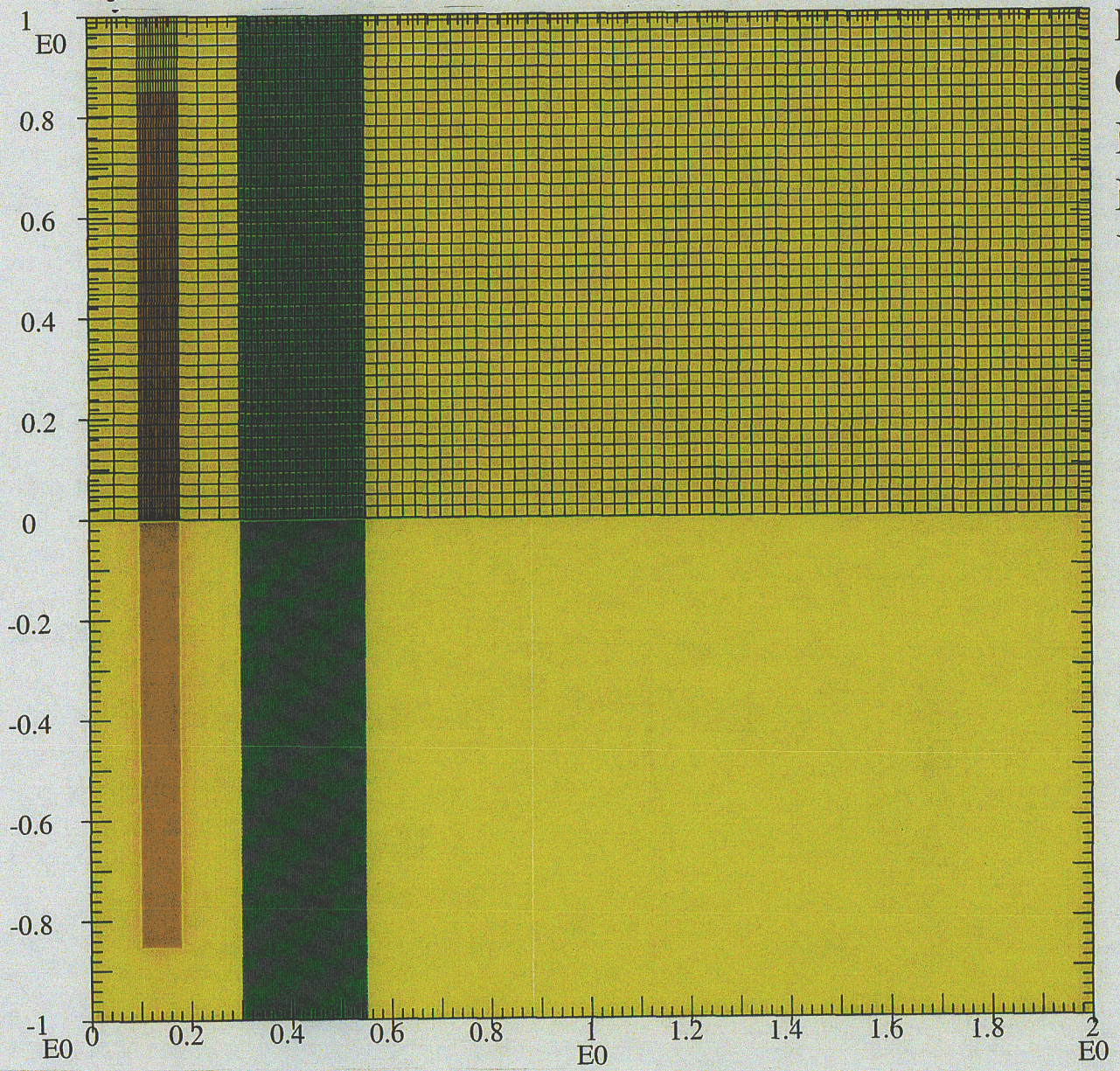

Red: projectile
Green: target
Blue: witness plate
Dark blue: LiF
Yellow: vacuum background

clpa--29-mg-6-19-2001

50

Figure 45

Second series CLP EOS experiments modeling calculations

Very fine zoning (405x337) witness plate and backing closeup at t=0

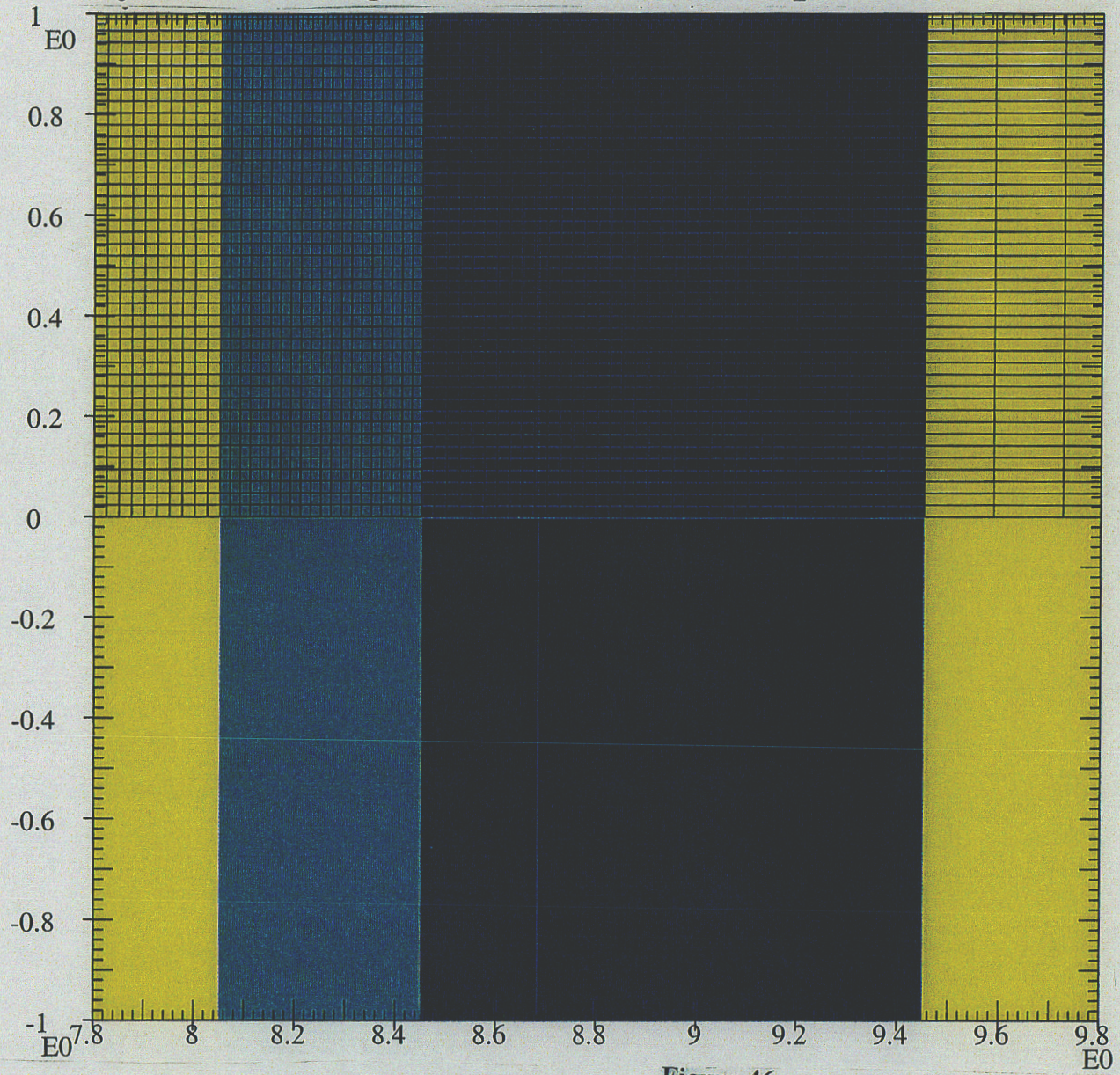

Blue: witness plate
Dark blue: LiF
Yellow: vacuum background

clpa--30-mg-6-19-2001

Figure 46

Second series CLP EOS experiments modeling calculations

Very fine zoning (405x337) 17mm dia. proj. at 6km/s: t=20μs

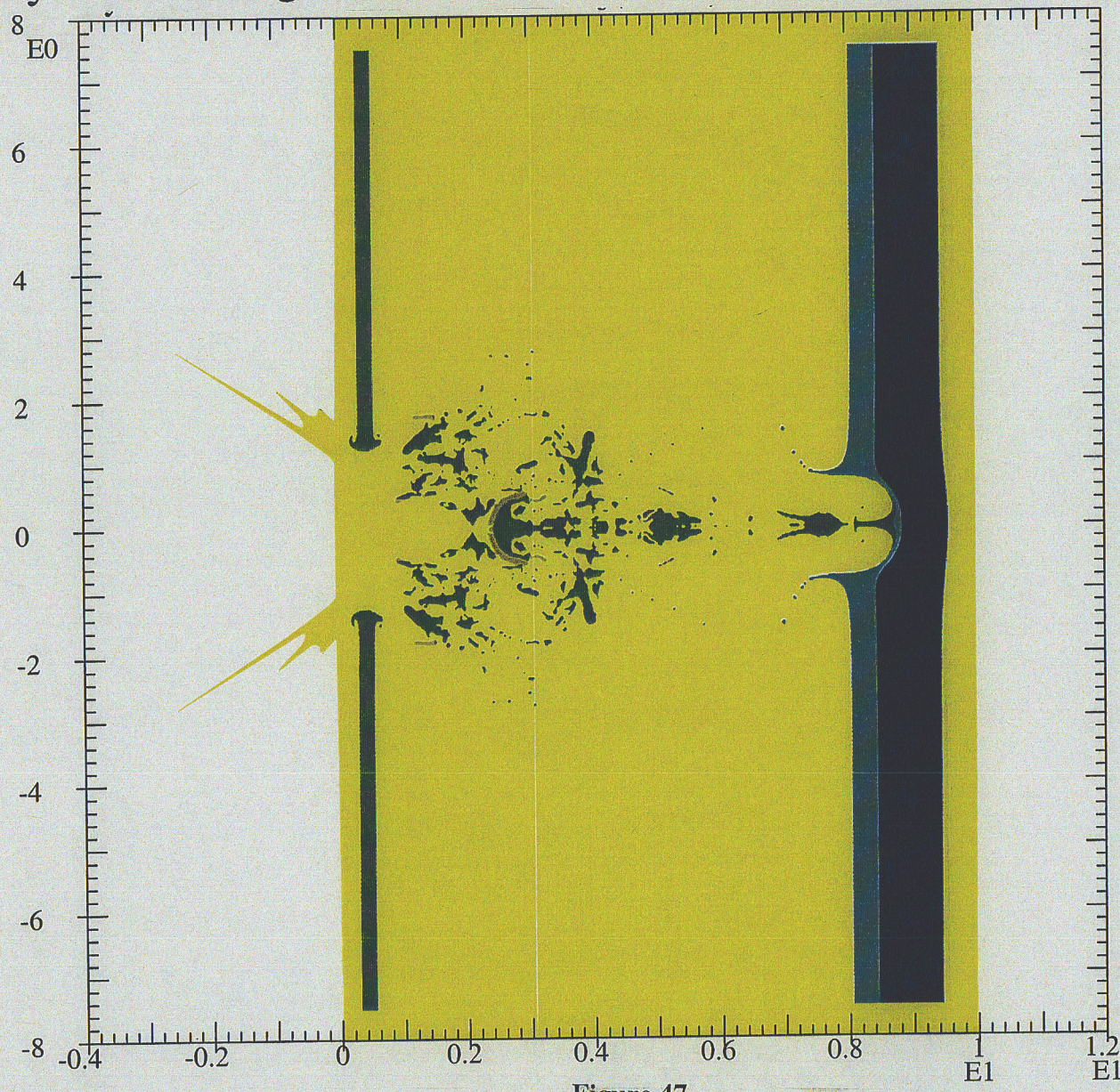

Red: projectile
Green: target
Blue: witness plate
Dark blue: LiF
Yellow: vacuum background

clpa--33-mg-6-26-2001

Figure 47

Second series CLP EOS experiments modeling calculations

Very fine zoning (405x337) 17mm diameter projectile at 6km/s

Particle velocities at rear of witness plate on axis and 2,4 and 6mm away

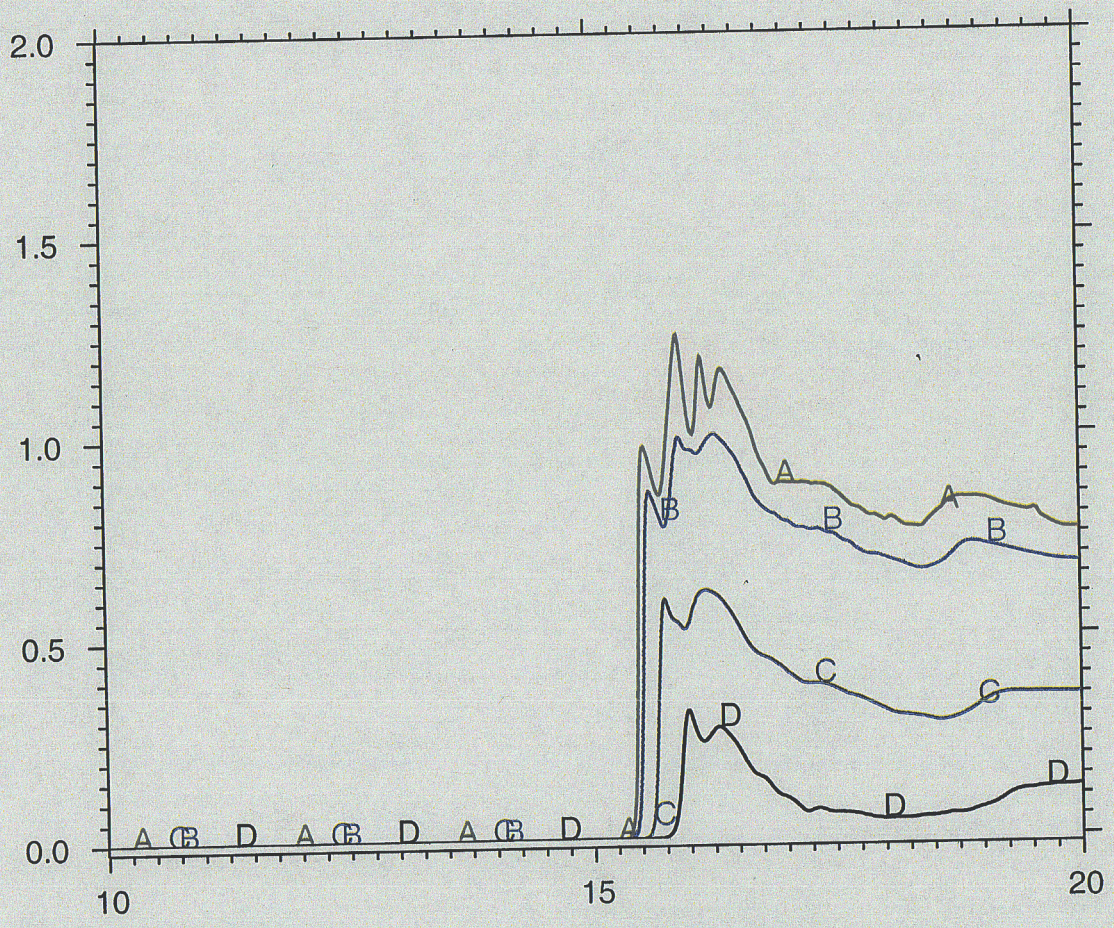

Particle velocity (km/s)

Time (μs)

Figure 48

clpa--34-mg-6-26-2001

Second series CLP EOS experiments modeling calculations

Very fine zoning (405x337) 17mm dia. proj. at 11km/s: t=10μs

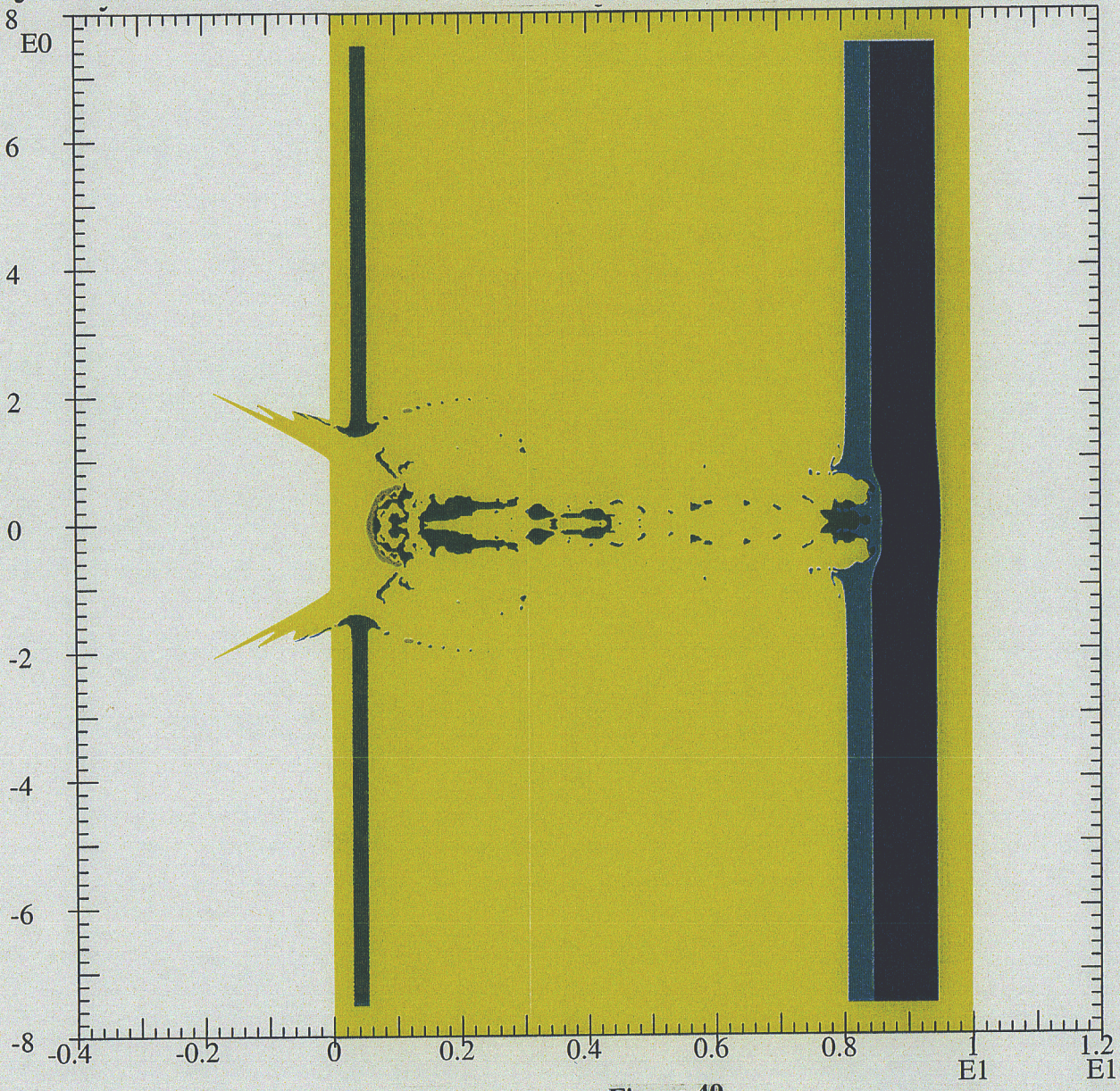

Red: projectile
Green: target
Blue: witness plate
Dark blue: LiF
Yellow: vacuum background

clpa--31-mg-6-26-2001

Figure 49

Second series CLP EOS experiments modeling calculations

Very fine zoning (405x337) 17mm diameter projectile at 11km/s
Particle velocities at rear of witness plate on axis and 2,4 and 6mm away

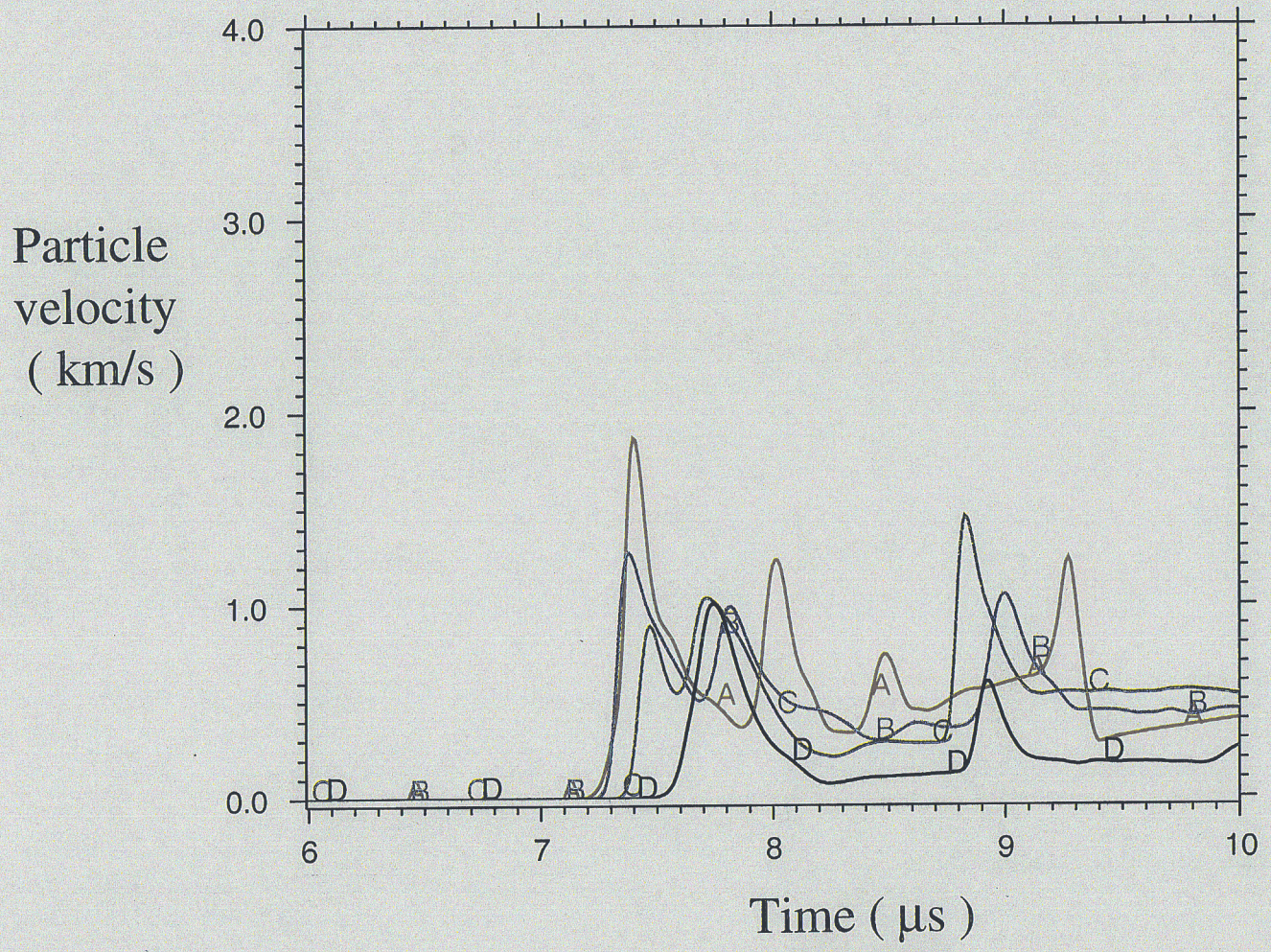

Figure 50

Second series CLP EOS experiments modeling calculations show particle velocity profile zoning dependence on axis

17mm diameter projectile at 6km/s particle velocity on axis at rear of witness plate

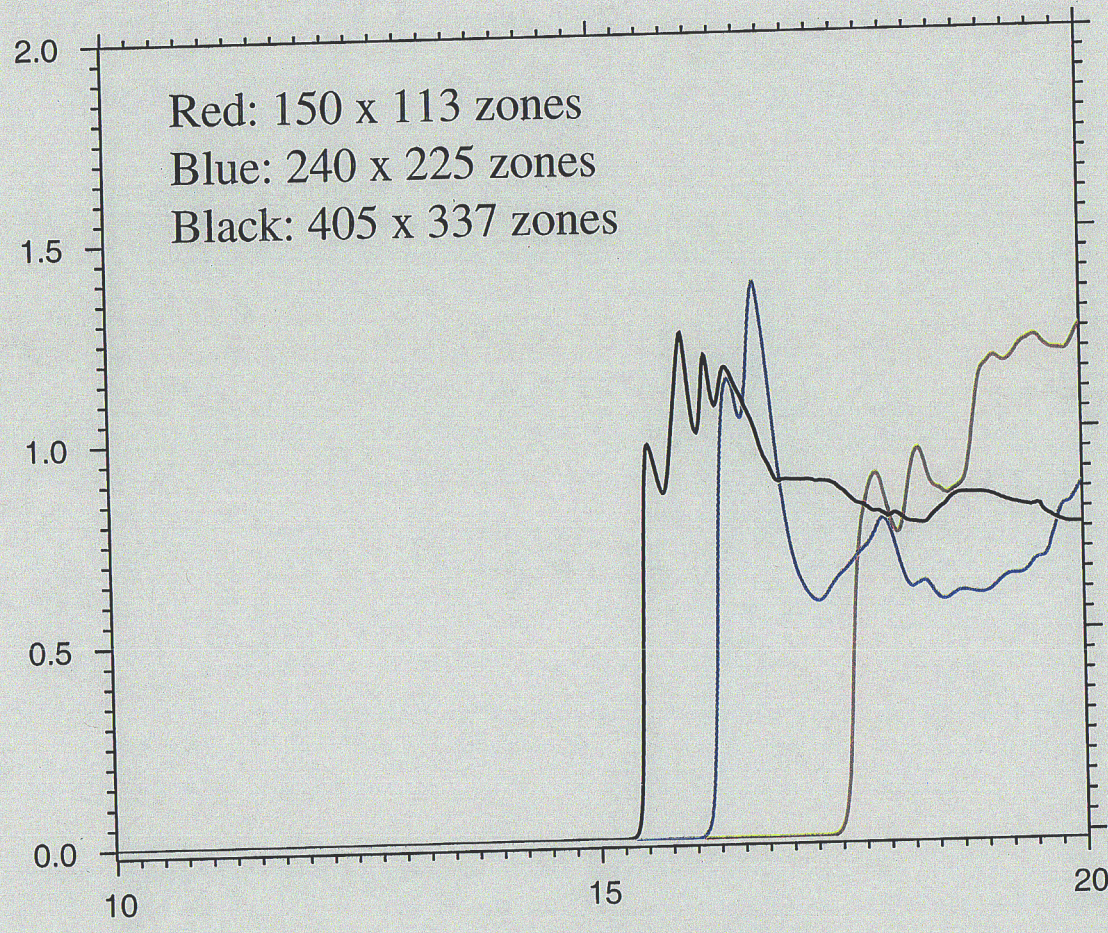

clpa--35b-mg-6-26-2001

Figure 51

Second series CLP EOS experiments modeling calculations show particle velocity zoning dependence on axis

17mm diameter projectile at 11km/s particle velocity on axis at rear of witness plate

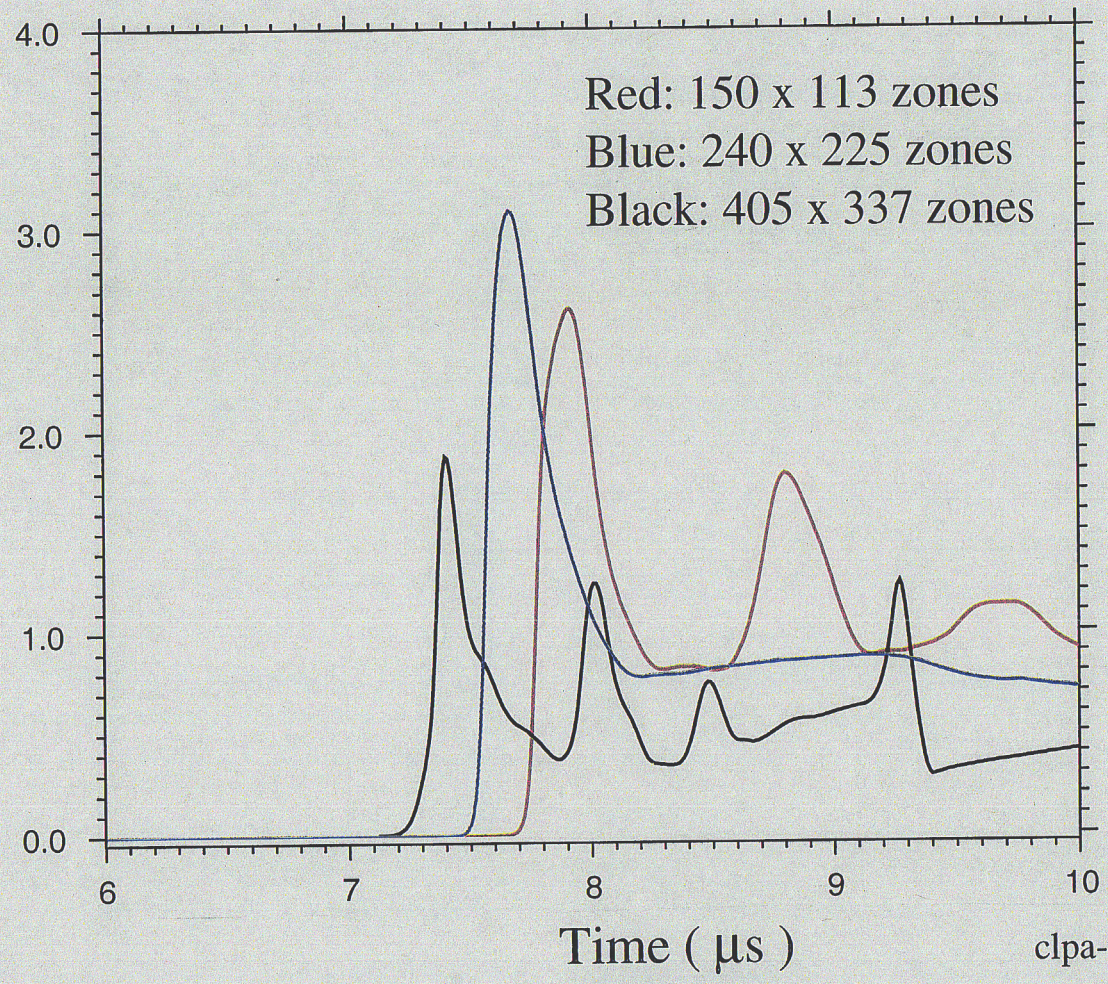

clpa--35-mg-6-19-2001

Figure 52